Fungal Diversity

Fungal Diversity (2026) 136: 136017
https://doi.org/10.65390/fdiv.2026.136017

Research Article

OPEN ACCESS

Absolute-quantitative microbiome profiling identifies pathogen-sensitive windows and cross-domain assembly rules in *Morchella* cultivation soils

Ying Chen[1#], Zong-Lin Deng[2#], Xue-Lian Cao[1#], Shi-Shi Liu[1], Jie Ou[3], Xiao-Rong Wang[2], Li-Xu Liu[1], Chang Tian[1], Tian-Li Li[2], Jie Tang[1*] and Li-Yuan Xie[1*]

[1]Sichuan Institute of Edible Fungi, National-Local Joint Engineering Laboratory of Breeding and Cultivation of Edible and Medicinal Fungi, Xindu Field Scientific Observation and Research Station of Agricultural Microorganisms-Ministry of Agriculture and Rural Affairs, Environment-friendly and Efficient Water-Saving Technology and Equipment for Hilly Agriculture Key Laboratory of Sichuan Province, Sichuan Academy of Agricultural Sciences, Chengdu 610066, China; [2]School of Life Science and Technology, University of Electronic Science and Technology of China, Chengdu 611731, China; [3]School of Information and Software Engineering, University of Electronic Science and Technology of China, Chengdu 611731, China

[#]These authors contributed equally to this work

***Corresponding authors:** xly_0226@126.com (L.-Y. X.); biotang@163.com (J. T.)

Received: 26 March 2026 / Accepted: 30 June 2026 / Published: 05 August 2026

Abstract

Although soilborne diseases severely threaten *Morchella* cultivation, the underlying quantitative microbial processes associated with disease outbreaks remain poorly understood. Here, we profiled high-resolution temporal dynamics across the full cultivation cycle of *Morchella sextelata* by integrating spike-in-calibrated amplicon sequencing with multidimensional ecological analyses. By overcoming the compositional constraints of traditional relative-abundance data, this approach revealed pronounced, stage-dependent shifts in bacterial 16S rRNA gene and fungal ITS copy-number abundances. We identified a potential disease-risk window spanning the Mycelial Growth Stage to Young Fruiting Body Stage (MGS–YGS), with a core transition phase during primordium formation and early fruiting (PFS–YGS). During this interval, fungal communities exhibited pronounced stage-dependent restructuring, increased network fluctuation, and significant enrichment of putative antagonistic or pathogen-associated genera, particularly *Fusarium* and *Lecanicillium*. Community assembly analyses revealed clear domain-specific patterns: bacterial succession was governed predominantly by homogeneous selection and exhibited cohesive, stable association structures, whereas fungal communities were highly responsive to host reproductive transitions and dynamic soil conditions. Environmental association analyses indicated that bacterial dynamics were linked primarily to relatively stable edaphic properties, such as pH, organic matter, and total nitrogen, whereas fungal succession was strongly coupled with labile nutrients and moisture, including available phosphorus, available potassium, and moisture content. Together, these findings provide a quantitative microbiome framework for identifying candidate disease-risk periods in *Morchella* cultivation soils and highlight fungal community dynamics as sensitive indicators of cultivation-stage transitions. This study advances microbiome-informed strategies for disease management and sustainable morel production.

Key words: Soil microbiome; Absolute quantification; Spike-in calibration; Candidate disease-risk window; Community assembly; Cross-domain network; *Morchella sextelata*

Citation: Chen, Y., Deng, Z.-L., Cao, X.-L., Liu, S.-S., Ou, J., Wang, X.-R., Liu, L.-X., Tian, C., Li, T.-L., Tang, J., Xie, L.-Y. (2026) Absolute-quantitative microbiome profiling identifies pathogen-sensitive windows and cross-domain assembly rules in *Morchella* cultivation soils. Fungal Diversity 136: 136017. https://doi.org/10.65390/fdiv.2026.136017

Introduction

Morels (*Morchella* spp.) are highly valued edible and medicinal fungi of significant economic importance, esteemed for their distinctive aroma, rich nutritional profile, and diverse bioactive properties (He et al. 2012; Liu et al. 2016; Kewlani et al. 2023; Wu et al. 2021; Zhang et al. 2023b). Recent advancements in artificial cultivation techniques have successfully transitioned morels from a seasonal wild delicacy into a high-value agricultural commodity amenable to large-scale production, establishing them as a prominent focal point in the global mushroom industry (Liu et al. 2018; Huang et al. 2024; Xu et al. 2024).

Unlike saprotrophic species such as *Lentinula edodes* and *Flammulina velutipes*, morels display greater complexity in both ecological strategy and developmental biology (Pion et al. 2013; Benucci et al. 2019; Du and Yang 2021; Tan et al.

2021; Yue et al. 2024; Deng et al. 2025a). Their life cycle spans multiple critical stages, including hyphal colonization, primordium initiation, fruiting-body development, and post-harvest senescence (Yan et al. 2025b). This process is highly dependent on dynamic interactions with the surrounding environment, particularly the rhizosphere or cultivation-substrate microbiota. A growing body of evidence indicates that soil microbial communities play pivotal roles in host health and reproductive success through processes such as organic-matter decomposition, nutrient mineralization, phytohormone modulation, and pathogen suppression (Cole et al. 2009; Quast et al. 2013; Orlofsky et al. 2021; Ban et al. 2023; Yu et al. 2022; Li et al. 2024). Specific functional guilds—such as plant-growth-promoting bacteria and antagonistic fungi—can further facilitate mycelial expansion or inhibit competing and pathogenic microorganisms via the production of secondary metabolites or signaling molecules (Chen et al. 2024; Yu et al. 2025).

High-throughput sequencing of bacterial 16S rRNA genes and fungal ITS regions has revealed stage-specific successional patterns of microbial communities in morel cultivation systems (Benucci et al. 2019; Zhang et al. 2023a; Yan et al. 2025a, b; Guo et al. 2025). However, most studies rely exclusively on relative-abundance data, which are compositionally constrained and highly sensitive to technical biases such as PCR amplification and sequencing-depth variability. Apparent increases in relative abundance may not reflect true microbial proliferation but rather reductions in other taxa, producing misleading impressions of enrichment. Such compositional artifacts can obscure key ecological processes—including pathogen colonization, community assembly, and functional dominance—and hinder accurate linkage of microbial dynamics with host physiology or disease emergence.

To overcome these limitations, spike-in-DNA-based absolute-quantification approaches have been developed. By introducing synthetic internal-reference sequences with known copy numbers into each sample prior to DNA extraction or amplification, these methods calibrate technical biases and enable precise estimation of absolute microbial abundances (Tourlousse et al. 2017; Vandeputte et al. 2017; Yang et al. 2018; Boshier et al. 2020; Doyle et al. 2025). Absolute quantification allows accurate tracking of microbial biomass, pathogen proliferation, and stage-specific community shifts, providing insights into microbial network stability, deterministic versus stochastic assembly, and responses to environmental filtering. Despite these advances, such approaches have not yet been applied to *Morchella* or comparable edible fungal cropping systems, leaving a critical gap in understanding the interplay between microbiome ecology, disease thresholds, and reproductive development.

Here, we coupled spike-in-calibrated quantitative profiling with integrative ecological analyses to construct a high-resolution successional atlas of the soil microbiome across the full cultivation cycle of *Morchella sextelata*. By integrating absolute gene-copy abundance estimates with phylogenetically informed community assembly metrics (βNTI), neutral community modeling, co-occurrence network analyses, and edaphic association profiling, we sought to identify potential disease-susceptibility windows and disentangle the domain-specific ecological processes shaping bacterial and fungal communities. This framework provides a quantitative ecological perspective on microbiome dynamics in morel cultivation soils and reveals marked fungal community reorganization during host reproductive development. Collectively, our findings establish a foundation for microbiome-informed disease management and sustainable production of cultivated morels.

Materials and methods

Cultivation conditions and sample processing

Morchella sextelata was cultivated during the 2023–2024 winter cropping season in a plastic greenhouse located in Xindu District, Chengdu, Sichuan Province, China (30.8230° N, 104.1757° E). The cultivation substrate consisted of locally sourced loamy soil amended with wheat straw and organic fertilizer and was pasteurized before sowing.

Before sowing, a permanent spatial sampling grid was established across the cultivation field. The grid consisted of nine fixed plots (2 m × 2 m each) that were uniformly distributed throughout the greenhouse. The positions of all plots were physically marked to ensure repeated sampling from the same spatial locations across all developmental stages.

Soil samples were collected at seven developmental stages: Pre-sowing Background Stage (PBS; November 15, 2023), Initial Establishment Stage (IES; December 10, 2023), Mycelial Growth Stage (MGS; January 5, 2024), Primordium Formation Stage (PFS; January 20, 2024), Young Fruiting Body Stage (YGS; February 20, 2024), Harvest Stage (HRS; March 15, 2024), and Post-harvest Recovery Stage (PRS; April 5, 2024). At each sampling time point, the upper approximately 2 cm of soil was removed, and root-zone soil from 2–8 cm depth, operationally defined as the soil fraction closely associated with morel mycelia, was collected using sterile augers.

At each developmental stage, samples were collected from the same set of nine fixed plots, regardless of whether fruiting bodies had emerged in a given plot at later stages. Within each plot, three soil cores were collected and pooled to generate one plot-level composite sample. To reduce the influence of micro-spatial heterogeneity and uneven fruiting patterns within the greenhouse, plot-level composite samples from every three spatially adjacent plots were physically combined and thoroughly homogenized. This procedure yielded three consolidated composite biological replicates per stage, resulting in 21 soil samples in total for soil physicochemical analysis and microbiome profiling. These 21 soil samples generated 42 microbial profiles, including 21 bacterial 16S rRNA gene profiles and 21 fungal ITS profiles. Sampling tools were sterilized with 70% ethanol between samples.

At each sampling time point, the fruiting status of each permanent plot was recorded, including primordium number, young fruiting body number, and mature fruiting body number where applicable. For the YGS and HRS stages, the fixed plots included plots actively producing fruiting bodies at the time of sampling. For earlier stages (PBS, IES, MGS, and PFS), when fruiting bodies had not yet emerged, samples were collected from the same fixed plots irrespective of their subsequent fruiting status. This design was intended to minimize spatial selection bias and to ensure that stage-to-stage comparisons primarily reflected temporal microbial succession.

After collection, consolidated soil samples were thoroughly homogenized and divided into subsamples. For microbiome analysis, aliquots were flash-frozen in liquid nitrogen and stored at –80 °C until DNA extraction. For physicochemical analysis, soil subsamples were air-dried, passed through a 2-mm sieve, and analyzed for pH, soil organic matter (SOM), total nitrogen (TN), total phosphorus (TP), total potassium (TK), alkaline-hydrolyzable nitrogen (AN), available phosphorus (AP), available potassium (AK), and moisture content (MC) following standard protocols. Dry soil mass was determined gravimetrically to normalize microbial gene-copy abundance estimates. Synthetic spike-in DNA was added to frozen soil samples before DNA extraction to calibrate downstream gene-copy abundance estimates.

DNA extraction, PCR amplification, and library construction

Total genomic DNA was extracted from 0.5 g of soil using a CTAB-based protocol optimized for complex environmental matrices (Liu et al. 2024). Before cell lysis, synthetic spike-in DNA sequences (GenStar Biosciences, catalog no. NGS-SPIKE-101) with known copy numbers (1×10^6 copies per 0.5 g soil) were added to each sample. These internal standards were used to account for potential DNA losses during extraction and PCR amplification and to enable spike-in-calibrated gene-copy abundance estimation.

The bacterial 16S rRNA V3–V4 region and fungal ITS1 region were amplified using universal primer pairs. All primers contained Illumina adapter overhangs to facilitate subsequent library construction. The full list of primer sequences, including target regions, sequences (5′→3′), and expected amplicon lengths, is provided in Supplementary Table S1.

PCR amplification was performed in 20 μL reactions containing 4 μL of 5× TransStart FastPfu buffer, 2 μL of dNTPs (2.5 mM each), 0.8 μL each of forward and reverse primers (5 μM), 0.4 μL of TransStart FastPfu DNA polymerase, 10 ng of extracted DNA template, and nuclease-free water to the final volume. Thermal cycling conditions were as follows: initial denaturation at 95 °C for 3 min; 27 cycles of denaturation at 95 °C for 30 s, annealing at 55 °C for 30 s, and extension at 72 °C for 30 s; followed by a final extension at 72 °C for 10 min and holding at 4 °C. All reactions were performed on an ABI GeneAmp® 9700 thermal cycler.

PCR products were separated by 2% agarose gel electrophoresis, and target amplicons were excised and purified using a PCR Clean-Up Kit. Purified amplicons were quantified using a Qubit 4.0 fluorometer (Thermo Fisher Scientific, USA).

Sequencing libraries were constructed using a rapid DNA-seq kit following the manufacturer's protocol. Library preparation included adapter ligation, magnetic bead-based size selection to remove adapter dimers, PCR enrichment of library templates, and final magnetic bead purification. Paired-end sequencing was performed on an Illumina NextSeq 2000 platform.

Bioinformatics and data analysis

Raw paired-end reads were demultiplexed according to their barcode sequences and quality-filtered using fastp (version 0.19.6). Reads were truncated using a sliding window of 50 bp when the average quality score within the window fell below 20. Reads shorter than 50 bp after trimming and reads containing ambiguous bases (N) were discarded. Quality-filtered paired-end reads were merged using FLASH (version 1.2.11), with a minimum overlap of 10 bp and a maximum mismatch ratio of 0.2 within the overlap region. Primer sequences were removed, and sequence orientations were adjusted before downstream analysis.

Amplicon sequence variant (ASV) inference was performed using the DADA2 plugin implemented in QIIME2 (version 2020.6) with default parameters. Taxonomic assignment was conducted using the Naïve Bayes classifier in QIIME2. Bacterial 16S rRNA gene sequences were classified against the SILVA database (version 138), whereas fungal ITS sequences were classified against the UNITE database (version 9.0). ASVs assigned to chloroplasts, mitochondria, or non-target lineages were removed before downstream analyses. Synthetic spike-in ASVs were identified by matching their sequences to the known synthetic spike-in reference sequences and were separated from biological ASVs before community analyses.

Spike-in calibration was performed using synthetic reference sequences with known input copy numbers. These spike-in references were used to establish sample-specific calibration relationships between observed spike-in read counts and known spike-in inputs, thereby enabling the conversion of biological ASV read counts into spike-in-calibrated gene-copy abundance estimates. The known copy numbers of spike-in standards were determined according to the following equation: Copy number (copies μL^{-1}) = [6.02×10^{23} × DNA concentration (ng μL^{-1}) × 10^{-9}] / [DNA length (bp) × 660].

For each sample, observed read counts of spike-in ASVs were related to their known input copy numbers. Both read counts and input copy numbers were $\log_{10}$-transformed, and the sample-specific calibration model was fitted as follows: $\log_{10}$ (copy number) = a × $\log_{10}$(read count) + b, where a and b represent the slope and intercept of the sample-specific calibration relationship, respectively. Calibration parameters, including slope, intercept, correlation coefficient (*r*), and p value, are provided in Supplementary Table S2 for 16S rRNA gene sequencing and Supplementary Table S3 for ITS sequencing. The raw read counts of spike-in ASVs are provided in Supplementary Table S4 for 16S rRNA gene sequencing and Supplementary Table S5 for ITS sequencing.

For each biological ASV, the spike-in-calibrated copy number was estimated from the corresponding sample-specific calibration relationship as follows: ASV copy number = 10^ [a × $\log_{10}$ (ASV read count) + b]. The copy number of each ASV was then normalized to dry soil mass using the following equation: ASV abundance (copies g^{-1} dry soil) = [M × ASV copy number] / [m × W], where M is the total amount of extracted DNA from the sample, m is the amount of DNA template used in the PCR reaction, and W is the dry-weight equivalent of soil used for DNA extraction. Taxon-level gene-copy abundances were obtained by summing the calibrated ASV-level copy numbers assigned to the same taxon. The resulting values represent spike-in-calibrated 16S rRNA gene or ITS copy-number estimates per gram of dry soil, rather than absolute microbial cell counts.

Diversity analyses

Alpha diversity was calculated after ASV tables were rarefied to a uniform sequencing depth. Shannon, Simpson, Chao1, and Faith's phylogenetic diversity (PD) indices were calculated using the q2-diversity plugin in QIIME2. Differences among developmental stages were evaluated using one-way ANOVA followed by Tukey's HSD test ($\alpha = 0.05$). Normality and homogeneity of variances were assessed using Shapiro–Wilk and Levene's tests, respectively. Given the limited sample size per stage ($n = 3$), non-parametric alternatives, including the Kruskal–Wallis test followed by Dunn's post hoc test, were also performed to confirm ANOVA results. No discrepancies between parametric and non-parametric approaches were observed for the reported alpha-diversity comparisons.

Beta diversity was assessed using Bray–Curtis dissimilarity matrices computed from spike-in-calibrated gene-copy abundance estimates. PERMANOVA was performed using the adonis2 function in the vegan R package with 999 permutations to test the effect of developmental stage. Homogeneity of multivariate dispersion was examined using betadisper. Non-metric multidimensional scaling (NMDS) was applied for visualization.

Co-occurrence network analysis

Co-occurrence networks were constructed using ASV-level spike-in-calibrated gene-copy abundance estimates. For each network, ASVs detected in fewer than 20% of the corresponding samples were excluded to reduce the influence of rare taxa. Spearman's rank correlations were calculated between retained ASVs, and significant correlations were retained as network edges using a threshold of $|\rho| > 0.6$ and FDR-adjusted $p < 0.05$.

Stage-specific bacterial and fungal networks were constructed separately for each developmental stage to characterize stage-associated association structures. Global bacterial and fungal networks were constructed using all samples within each domain across the full cultivation cycle. The integrated cross-domain bacterial–fungal network was constructed from paired bacterial and fungal profiles, comprising 21 bacterial 16S rRNA gene profiles and 21 fungal ITS profiles derived from the same 21 soil samples. A *Morchella*-centered subnetwork was extracted from the integrated cross-domain network to identify bacterial and fungal ASVs directly or indirectly associated with *Morchella*. Positive and negative fungal association networks were further generated for dominant fungal taxa to visualize stage-associated positive and negative correlations around *Morchella*.

All networks were analyzed using the igraph package in R. Network topological metrics, including node number, edge number, mean degree, clustering coefficient, and modularity, were calculated. Network modules were detected using the Louvain algorithm.

Community assembly analyses

Stochastic assembly processes were assessed by fitting the Sloan neutral community model using the neutral.fit function in the MicEco R package. Model fit (R^2) and migration rate (Nm) were used to quantify the influence of neutral processes.

Deterministic and stochastic contributions to phylogenetic turnover were evaluated using the β-nearest taxon index (βNTI) with 999 phylogenetic randomizations. $\beta NTI > +2$ indicated heterogeneous selection, $\beta NTI < -2$ indicated homogeneous selection, and $|\beta NTI| < 2$ indicated stochastic dominance (Stegen et al. 2013; Ning et al. 2019).

Differential abundance and biomarker identification

Linear discriminant analysis effect size (LEfSe) analysis was used to identify taxa differentially abundant across developmental stages. Features were first screened using the Kruskal–Wallis test ($p < 0.05$), followed by linear discriminant analysis to estimate effect sizes. Taxa with LDA scores ≥ 2.0 ($\log_{10}$) were considered stage-associated biomarkers. This approach integrates statistical significance with effect size to prioritize taxa with consistent and meaningful stage-associated enrichment.

Linking microbial communities with soil properties

Associations between microbial community composition and soil physicochemical variables, including pH, SOM, TN, TP, TK, AN, AP, AK, and MC, were assessed using Mantel tests with 999 permutations in the vegan R package. Bray–Curtis dissimilarity was used for microbial communities, and Euclidean distance was used for soil variables. This non-parametric approach does not assume normality of the underlying data and is robust to non-Gaussian distributions, restricted ranges of variation, and limited sample sizes.

Redundancy analysis (RDA) was performed on Hellinger-transformed spike-in-calibrated gene-copy abundance estimates. Environmental variables were centered and scaled. Multicollinearity among variables was evaluated using variance inflation factors (VIF), and variables with VIF > 10 were excluded from the final model. The significance of retained variables was tested using envfit with 999 permutations. Only variables that passed both VIF filtering and permutation testing ($p < 0.05$) were interpreted as soil variables significantly associated with microbial community structure. Variables with limited temporal variation across stages or non-significant community associations were excluded from interpretation.

All statistical analyses were performed in R version 4.2.0 (R Core Team, 2022). The significance threshold was set at $\alpha = 0.05$ for all tests unless otherwise specified.

Results

High-resolution soil microbial succession revealed by spike-in-calibrated quantification

To resolve microbial succession across the *Morchella* cultivation cycle, root-zone soil samples were collected from seven developmental stages, spanning the Pre-sowing Background Stage (PBS) to the Post-harvest Recovery Stage (PRS) (Fig. 1a). In parallel, nine soil physicochemical variables—pH, soil organic matter (SOM), total nitrogen (TN), total phosphorus (TP), total potassium (TK), alkaline-hydrolyzable nitrogen (AN), available phosphorus (AP), available potassium (AK), and moisture content (MC)—were measured to characterize the environmental context of each stage (Fig. 1b). Microbial communities were profiled using a spike-in-calibrated workflow, allowing conventional relative

abundance patterns to be compared with spike-in-calibrated gene-copy abundance estimates (Fig. 1c).

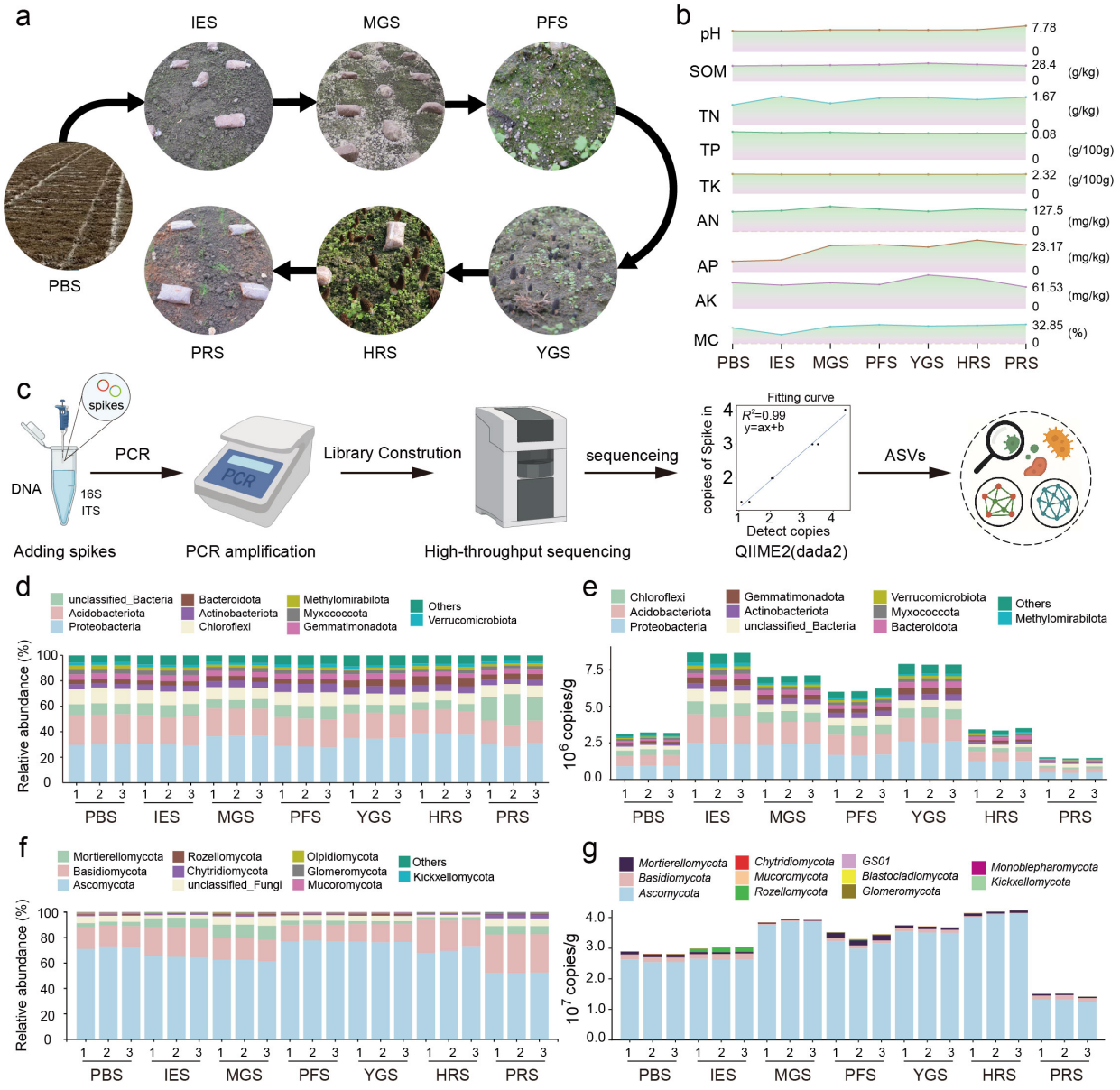

Fig. 1 Experimental design, soil physicochemical profiles, and spike-in-calibrated microbial abundance profiles. Seven developmental stages of *Morchella sextelata* cultivation were sampled: Pre-sowing Background Stage (PBS), Initial Establishment Stage (IES), Mycelial Growth Stage (MGS), Primordium Formation Stage (PFS), Young Fruiting Body Stage (YGS), Harvest Stage (HRS), and Post-harvest Recovery Stage (PRS) (a). Soil physicochemical variables included pH, soil organic matter (SOM), total nitrogen (TN), total phosphorus (TP), total potassium (TK), alkaline-hydrolyzable nitrogen (AN), available phosphorus (AP), available potassium (AK), and moisture content (MC) (b). The spike-in-calibrated workflow included DNA extraction with synthetic spike-in controls, PCR amplification of bacterial 16S rRNA gene and fungal ITS regions, library construction, high-throughput sequencing, and ASV (amplicon sequence variant) inference using QIIME2/DADA2 (c). Relative abundance profiles of bacterial and fungal phyla are shown in (d) and (f), respectively, whereas spike-in-calibrated gene-copy abundance estimates are shown in (e) and (g), respectively.

For bacterial communities, relative abundance profiles showed that Proteobacteria and Acidobacteriota were consistently dominant across the cultivation cycle, together accounting for more than half of the bacterial community at most stages (Fig. 1d). This relative-abundance view suggested only moderate compositional variation among developmental stages. In contrast, spike-in-calibrated gene-copy abundance profiles revealed more pronounced stage-dependent changes in bacterial taxa (Fig. 1e). Acidobacteriota increased after the Initial Establishment Stage (IES), reached relatively high gene-copy abundance during the Primordium Formation Stage (PFS) and Young Fruiting Body Stage (YGS), and declined thereafter. Actinobacteriota showed a contrasting pattern, with reduced gene-copy abundance after the Harvest Stage (HRS). These patterns indicate that several bacterial phyla underwent quantitative shifts that were less apparent in relative abundance profiles.

Fungal communities exhibited an even stronger contrast between relative abundance and spike-in-calibrated gene-copy abundance profiles. In the relative-abundance data, Ascomycota and Basidiomycota were the dominant fungal phyla throughout the cultivation cycle, and their proportional abundances appeared relatively stable among stages (Fig. 1f). However, spike-in-calibrated gene-copy abundance estimates revealed substantial quantitative reorganization of the fungal community (Fig. 1g). Ascomycota increased markedly from early cultivation stages toward HRS, coinciding with the expansion of *Morchella* during reproductive development, whereas Basidiomycota remained low in gene-copy abundance despite its apparent contribution in relative profiles. Thus, relative abundance alone underestimated the magnitude of fungal ITS copy-number accumulation during the cultivation cycle.

Together, these results show that relative abundance profiles can obscure major quantitative shifts in soil microbial communities. Although bacterial and fungal phyla appeared comparatively stable in proportional composition, spike-in-calibrated estimates revealed stage-dependent changes in 16S rRNA gene and ITS copy numbers. This distinction was particularly important for fungi, where the reproductive expansion of *Morchella*-associated Ascomycota strongly reshaped gene-copy abundance patterns without necessarily producing equivalent proportional changes. The spike-in-calibrated framework therefore provided a more quantitative basis for interpreting microbial succession in *Morchella* cultivation soils.

Temporal dynamics and resilience of soil bacterial communities

Bacterial alpha diversity varied across developmental stages (Fig. 2a). Richness, as indicated by Chao1, and phylogenetic diversity, as indicated by Faith's PD, were highest at the Initial Establishment Stage (IES), suggesting the presence of a relatively diverse and phylogenetically broad bacterial community during early establishment. Both indices declined at the Mycelial Growth Stage (MGS), coinciding with rapid *Morchella* mycelial expansion, and then partially recovered during the Young Fruiting Body Stage (YGS). Shannon and Simpson indices showed similar but less pronounced temporal variation, with relatively high values at the Pre-sowing Background Stage (PBS) and IES, a decline at MGS, and partial recovery toward the later stages. These patterns indicate that bacterial diversity was temporarily reduced during active mycelial growth but was not completely lost during the cultivation cycle.

Beta-diversity analysis further revealed moderate stage-associated shifts in bacterial community composition (Fig. 2b). Non-metric multidimensional scaling (NMDS) based on Bray–Curtis dissimilarity showed partial separation among developmental stages, although the relatively high stress value (stress = 0.2507) indicates that the ordination should be interpreted cautiously. PBS, IES, and MGS samples were positioned relatively close to one another, suggesting broadly similar bacterial composition during early vegetative development. In contrast, samples from the Primordium Formation Stage (PFS) and YGS were more dispersed, consistent with increased community variability during the transition to reproductive development. PRS samples tended to separate from earlier stages, suggesting post-harvest bacterial reorganization. Overall, the partial overlap among stages indicates that bacterial communities changed over time but retained a relatively stable compositional core.

Taxonomic patterns based on spike-in-calibrated gene-copy abundance profiles further supported stage-associated bacterial dynamics (Fig. 2c–f). At the phylum level, Verrucomicrobiota and Actinobacteriota showed increased gene-copy abundance around MGS and PFS, coinciding with mycelial growth and primordium formation (Fig. 2c, d). Gemmatimonadota and Cyanobacteriota were relatively enriched during YGS and HRS, suggesting that bacterial taxa differed in their responses to fruiting-stage environmental conditions (Fig. 2e). LEfSe analysis at the family level identified several stage-associated bacterial biomarkers (Fig. 2f). Streptomycetaceae and Vicinamibacteraceae were enriched in PBS and early cultivation stages, whereas Anaerolineaceae, Longimicrobiaceae, and Nocardioidaceae were associated with PRS, a stage characterized by post-harvest turnover and decomposition of residual organic matter.

Collectively, these results show that bacterial communities underwent measurable diversity, compositional, and taxonomic shifts during *Morchella* cultivation. Nevertheless, the magnitude of these shifts was relatively moderate, and bacterial communities retained substantial overlap among developmental stages. This pattern suggests that soil bacterial assemblages maintained a relatively resilient community structure across the cultivation cycle, potentially reflecting environmental buffering, functional redundancy, and the persistence of generalist bacterial taxa.

Stage-dependent fungal restructuring and enrichment of putative antagonistic taxa during reproduction

Fungal alpha diversity varied across developmental stages (Fig. 3a). Shannon and Simpson indices were highest at the Pre-sowing Background Stage (PBS), indicating relatively high community evenness before sowing, and then declined toward the Harvest Stage (HRS), followed by partial recovery during the Post-harvest Recovery Stage (PRS). In contrast, richness-related indices, including Chao1 and Faith's phylogenetic diversity (PD), were highest at the Initial Establishment Stage (IES) and remained relatively elevated around the Primordium Formation Stage (PFS), but decreased during later developmental stages. The lowest fungal diversity was observed at HRS, coinciding with the strong expansion of *Morchella* during fruiting. These patterns suggest that fungal community diversity was progressively compressed during reproductive development, particularly when *Morchella* became dominant.

Beta-diversity analysis revealed clear stage-associated differences in fungal community composition (Fig. 3b). NMDS ordination based on Bray–Curtis dissimilarity showed stronger separation among developmental stages than that observed for bacterial communities, with a relatively low stress value (stress = 0.187). PERMANOVA further supported a significant stage effect on fungal community composition ($R^2 = 0.571$, $p = 0.001$). PBS and PRS samples were positioned toward the negative side of NMDS1, whereas IES and HRS samples were separated toward the positive side. PFS occupied an intermediate position, suggesting a transitional community state. MGS and YGS were mainly separated along

NMDS2, indicating distinct fungal community configurations during mycelial growth and early fruiting. These patterns point to a pronounced phase of fungal compositional turnover spanning the transition from MGS to YGS and extending toward HRS.

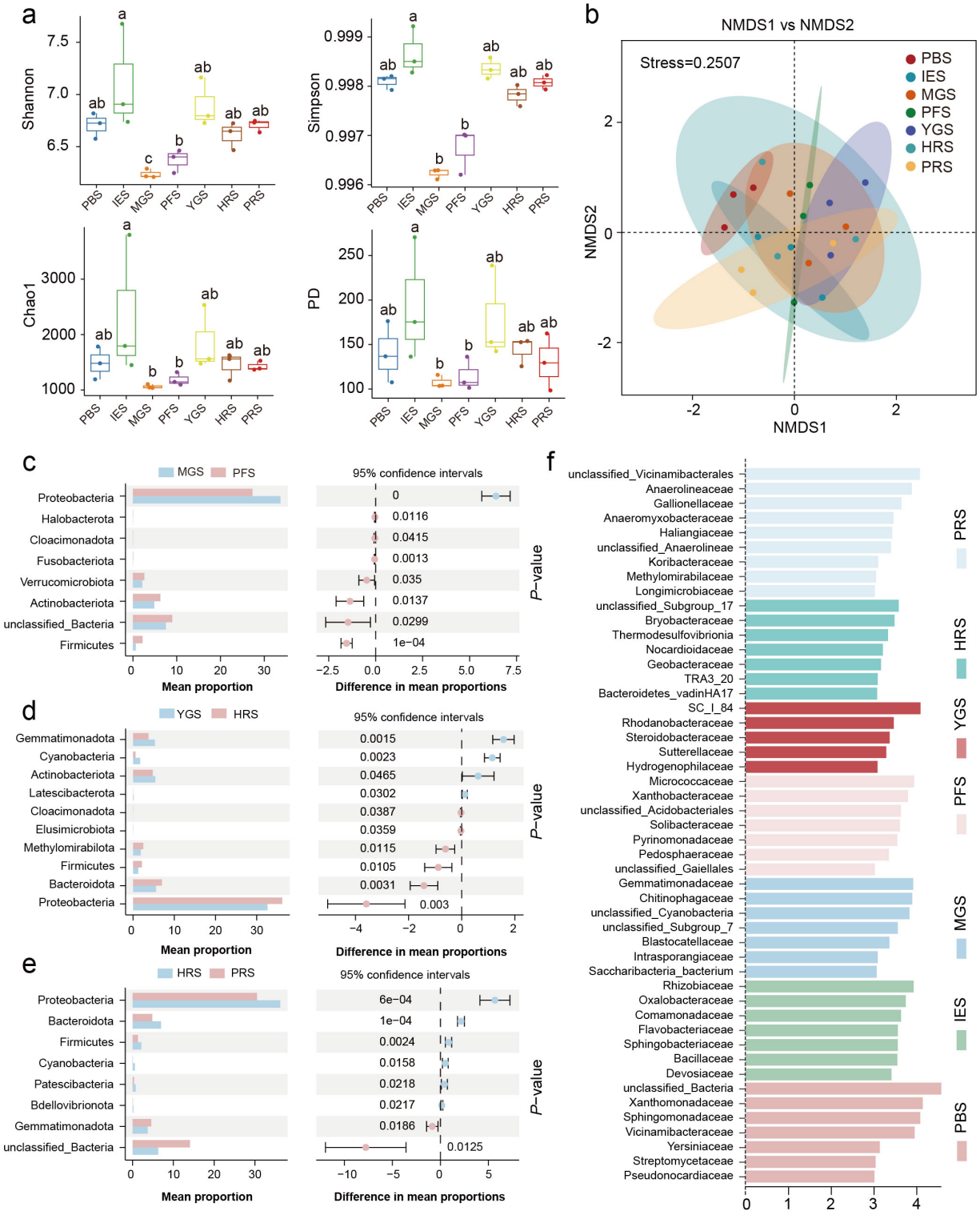

Fig. 2 Spike-in-calibrated bacterial community dynamics across *Morchella* cultivation stages. Alpha diversity indices, including Shannon, Simpson, Chao1, and Faith's phylogenetic diversity (PD), were compared across the seven developmental stages (a). Different letters above boxplots indicate significant differences among stages based on Tukey's HSD test ($p < 0.05$). NMDS (non-metric multidimensional scaling) ordination based on Bray–Curtis dissimilarities showed moderate stage-associated variation in bacterial community composition (b; stress = 0.2507). Differential abundance analyses at the phylum level are shown for representative stage comparisons, including MGS vs. PFS, YGS vs. HRS, and HRS vs. PRS (c–e). LEfSe (linear discriminant analysis effect size) analysis identified stage-associated bacterial biomarkers at the family level (f).

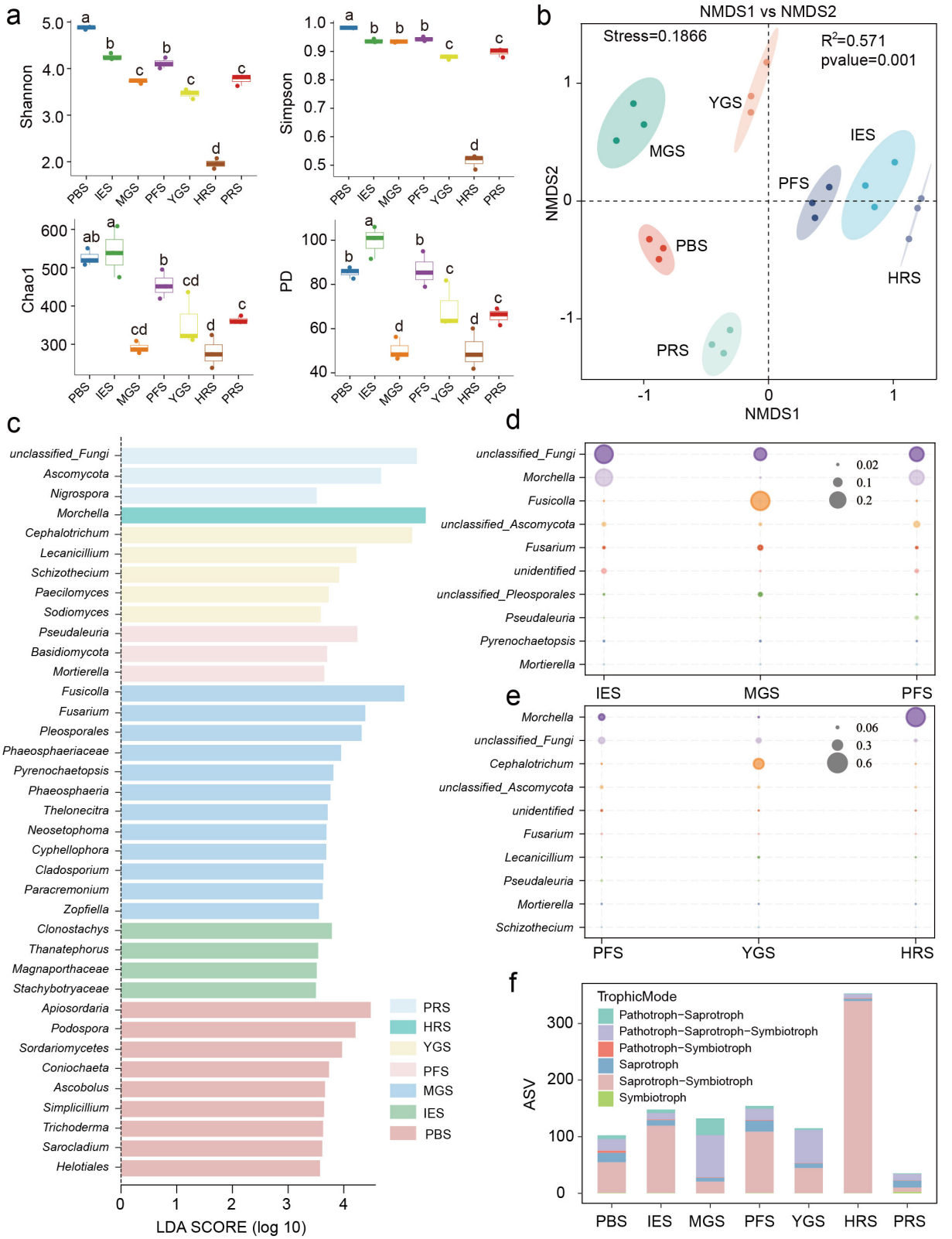

Fig. 3 Spike-in-calibrated fungal community dynamics across *Morchella* cultivation stages. Alpha diversity indices, including Shannon, Simpson, Chao1, and Faith's phylogenetic diversity (PD), were compared across the seven developmental stages (a). Different letters above boxplots indicate significant differences among stages based on Tukey's HSD test ($p < 0.05$). NMDS ordination based on Bray–Curtis dissimilarities showed stage-associated separation of fungal communities (b; stress = 0.1866; PERMANOVA $R^2 = 0.571$, $p = 0.001$). LEfSe (linear discriminant analysis effect size) analysis identified stage-associated fungal biomarkers across multiple taxonomic levels (c). Differential abundance analyses show representative fungal taxa enriched at selected developmental stages (d, e). Putative functional annotation of fungal ASVs by trophic mode revealed shifts among saprotrophs, symbiotrophs, pathotrophs, and mixed trophic guilds during cultivation (f).

Stage-associated biomarker analysis using LEfSe identified multiple fungal taxa enriched at different developmental stages (Fig. 3c–e). PBS was characterized by saprotrophic lineages, including Sordariomycetes, *Podospora*, and *Apiosordaria*. During IES, taxa such as *Clonostachys*, *Thanatephorus*, Magnaporthaceae, and Stachybotryaceae were enriched, suggesting an early colonization phase involving both saprotrophic and potentially antagonistic fungi. At MGS, *Fusicolla* and *Fusarium* were enriched, indicating the emergence of fungal taxa often associated with competitive or disease-related interactions in soil systems. PFS was associated with taxa such as *Pseudaleuria*, Basidiomycota, and *Mortierella*, which may reflect shifts in saprotrophic activity and microenvironmental conditions during primordium formation. During YGS, *Cephalotrichum*, *Lecanicillium*, *Schizothecium*, *Paecilomyces*, and *Sodiomyces* were enriched, indicating continued restructuring of the fungal community during early fruiting. At HRS, *Morchella* became overwhelmingly dominant, accounting for more than 90% of the fungal community, whereas PRS was characterized by increased representation of unclassified fungi and broader Ascomycota lineages, consistent with a post-harvest successional phase.

Differential abundance patterns further supported these stage-associated trends (Fig. 3d, e). *Fusicolla* and *Cephalotrichum* showed elevated abundance around MGS, whereas *Morchella* increased sharply from PFS and became dominant at HRS. Several putative antagonistic or pathogen-associated genera, including *Fusarium* and *Lecanicillium*, were detected during the MGS–YGS interval, suggesting that this broader developmental window may represent a period of increased biotic association changes and potential disease risk. However, because pathogenic potential was inferred from taxonomic identity rather than direct pathogenicity assays, these taxa should be interpreted as candidate risk-associated fungi rather than confirmed causal agents.

Functional guild profiling provided further support for stage-dependent fungal restructuring (Fig. 3f). Saprotroph–symbiotroph taxa constituted the dominant trophic guild across most developmental stages and increased markedly at HRS, consistent with the dominance of *Morchella* during fruiting. In contrast, mixed guilds containing pathotrophic components, such as pathotroph–saprotroph–symbiotroph groups, were enriched during the PFS–YGS interval. This pattern suggests that primordium formation and early fruiting represent a core phase of intensified fungal association changes within the broader MGS–YGS candidate disease-risk window.

Overall, fungal communities showed strong stage dependence during *Morchella* cultivation, including reduced diversity at HRS, pronounced compositional turnover during reproductive development, and enrichment of putative antagonistic or pathogen-associated taxa during MGS–YGS. These results suggest that fungal community profiles may serve as sensitive indicators of cultivation-stage transitions and potential disease-risk periods in *Morchella* production systems.

Distinct assembly patterns of bacterial and fungal communities during *Morchella* cultivation

To evaluate the relative contributions of neutral and niche-based assembly dynamics to microbial succession across the *Morchella* growing season, we fitted the neutral community model (NCM) and quantified phylogenetic turnover using the β-nearest taxon index (βNTI) (Fig. 4). Bacterial community assembly exhibited a strong fit to the NCM (R^2 = 0.866; 154 taxa; Fig. 4a), indicating that dispersal and drift-like processes contributed substantially to bacterial abundance–occurrence patterns. However, βNTI values consistently remained below −2 across all developmental stages (Fig. 4c), suggesting that bacterial phylogenetic turnover was predominantly structured by homogeneous selection. Collectively, these results indicate that neutral-like occurrence patterns were embedded within a phylogenetically constrained species pool shaped by strong and relatively uniform environmental filtering.

In contrast, the fungal community showed a moderate fit to the NCM (R^2 = 0.703; 522 taxa; Fig. 4b), indicating a comparatively greater deviation from neutral expectations. βNTI values for fungi exhibited a wider and more variable distribution than those observed for bacteria, with frequent departures beyond the stochastic threshold (|βNTI| > 2), particularly during the Primordium Formation Stage (PFS) and Young Fruiting Body Stage (YGS) (Fig. 4d). These patterns suggest that while homogeneous selection remained an important structuring force, additional stage-specific deterministic processes likely contributed to fungal community differentiation during host developmental transitions.

Taken together, these complementary analyses reveal distinct, domain-specific assembly regimes in morel cultivation soils. The bacterial domain maintained a relatively stable, environmentally filtered structure in which neutral-like occurrence patterns emerged within a phylogenetically constrained framework. In contrast, the mycobiome exhibited a more variable assembly regime, characterized by increased contributions of deterministic processes and heightened responsiveness to host developmental stages and associated microenvironmental shifts. These findings underscore the importance of integrating abundance–occurrence models with phylogenetic turnover metrics to better resolve microbial successional dynamics in cultivated morel systems.

Cross-domain networks reveal distinct bacterial and fungal association patterns

To elucidate microbial association patterns during *Morchella* cultivation, we reconstructed ASV-level co-occurrence networks for bacterial, fungal, and integrated bacterial–fungal cross-domain assemblages (Fig. 5). Global networks were first established across the entire cultivation cycle using the 21 profiles within each domain to capture baseline domain-specific topological structures, while stage-specific networks resolved temporal variation in network organization.

The global bacterial network contained 282 nodes and 1,939 edges (Fig. 5a), revealing a highly cohesive and densely connected topological backbone. Similarly, stage-specific bacterial networks exhibited consistently high connectivity, containing 287–319 nodes and 8,986–11,590 edges (Fig. 5b–h). This robust and persistent topology suggests that bacterial taxa maintained stable, highly connected association structures throughout morel development, consistent with phylogenetic assembly patterns (βNTI) indicating strong and relatively uniform homogeneous selection.

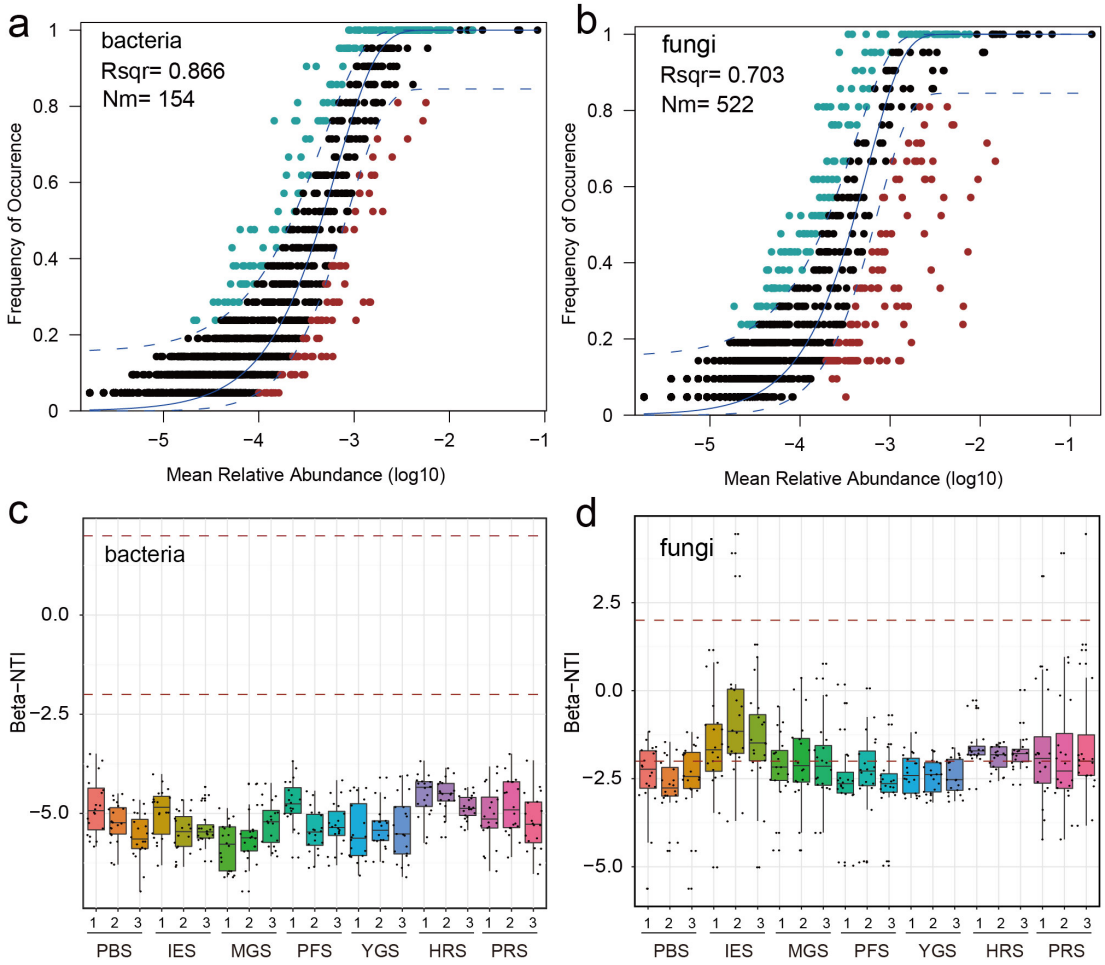

Fig. 4 Neutral model fitting and community assembly processes. Sloan neutral community model fitting shows the relationship between mean relative abundance (log_{10}-transformed) and occurrence frequency for bacterial (a) and fungal (b) communities. Solid lines indicate the best-fit neutral model, and dashed lines indicate the 95% confidence intervals. R^2 denotes goodness of fit, and Nm represents the estimated migration rate. βNTI (β-nearest taxon index) analysis shows phylogenetic assembly patterns for bacterial (c) and fungal (d) communities across the seven developmental stages. Dashed horizontal lines at βNTI = ±2 indicate deterministic thresholds: βNTI < −2 indicates homogeneous selection, βNTI > +2 indicates heterogeneous selection, and |βNTI| < 2 indicates stochastic processes.

In contrast, fungal networks were substantially smaller and structurally more variable. The global fungal network comprised 93 nodes and 357 edges (Fig. 5i), while stage-specific fungal networks contained 82–97 nodes and 766–1,257 edges (Fig. 5j–p). Compared with bacteria, fungal co-occurrence structures exhibited greater temporal variability, particularly during the Primordium Formation Stage (PFS) and Young Fruiting Body Stage (YGS). During these reproductive transitions, fungal networks showed reduced connectivity and pronounced structural fluctuations, suggesting increased responsiveness of fungal communities to host developmental stages and associated microenvironmental shifts. Partial recovery of fungal network structure was observed at the Post-harvest Recovery Stage (PRS), consistent with post-harvest community reorganization.

To capture cross-domain interactions, we reconstructed an integrated global network from 42 paired profiles (21 bacterial 16S rRNA gene and 21 fungal ITS datasets) derived from the same 21 soil samples (Fig. 5q). In this multi-kingdom network, bacterial ASVs formed a densely interconnected core, whereas fungal ASVs were less connected and positioned more peripherally. This asymmetric topology suggests that bacterial lineages represent a major structural component of the soil microbiome, while fungal lineages exhibit more variable and stage-associated association patterns.

A Morchella-centered subnetwork (Fig. 5r) identified several bacterial genera directly or indirectly associated with morel ASVs, including *Flavobacterium*, *Phyllobacterium*, *Duganella*, *Paenibacillus*, *Streptomyces*, *Kitasatospora*, *Mucilaginibacter*, *Polaromonas*, and *Cellvibrio*. These taxa constitute a candidate *Morchella*-associated bacterial consortium. Notably, several fungal genera previously reported as antagonistic or potentially pathogen-associated, including *Fusarium* and *Trichoderma*, were not embedded within the main *Morchella*-associated bacterial module but instead occurred in peripheral fungal network components (Fig. 5r). This spatial segregation suggests potential niche differentiation or indirect antagonistic associations between the core *Morchella* microbiome and these fungal lineages, although functional validation will be required to confirm these relationships.

In summary, co-occurrence network analyses reveal contrasting organizational patterns between soil bacterial

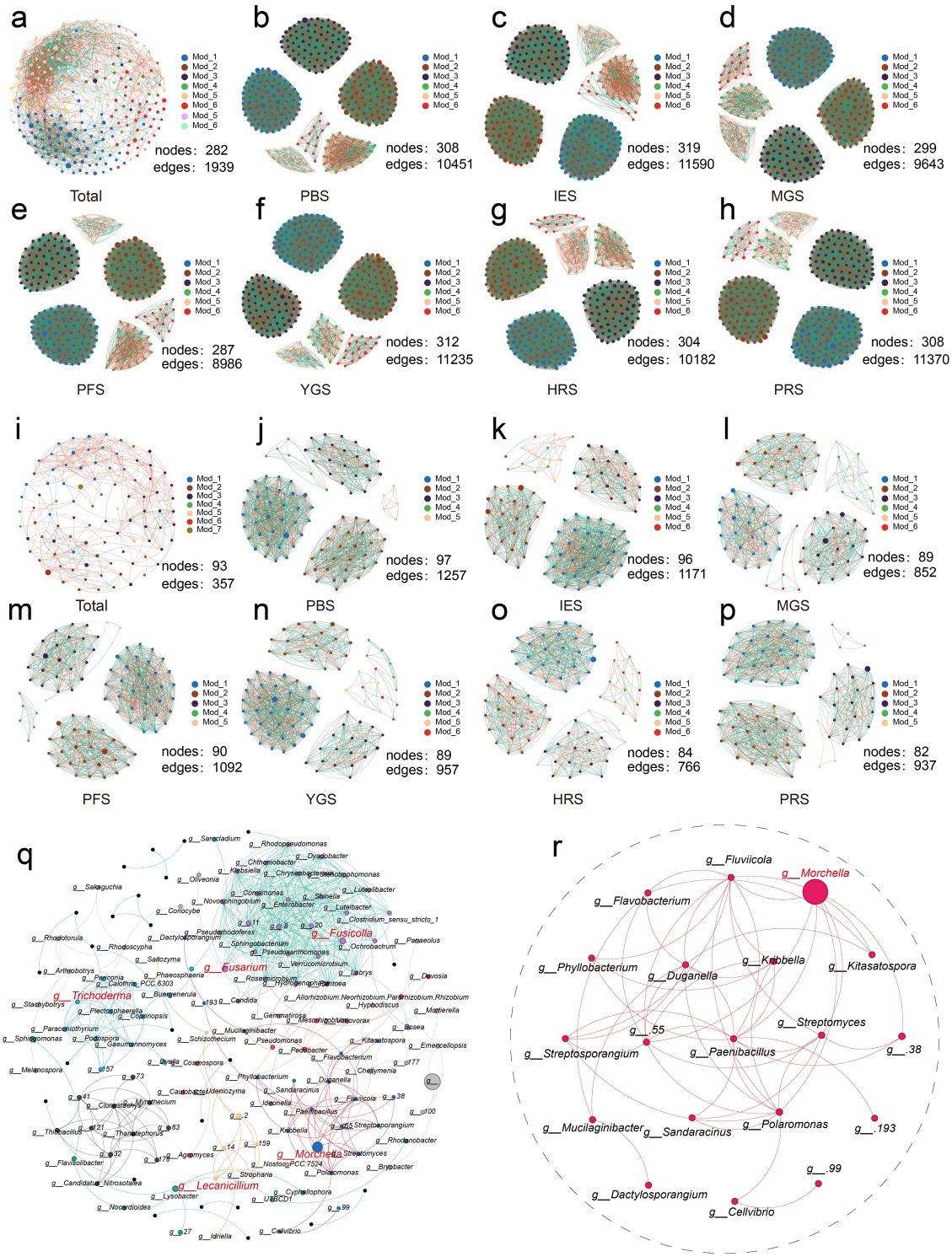

Fig. 5 Co-occurrence network structures of bacterial, fungal, and cross-domain communities. Networks were constructed based on ASV-level spike-in-calibrated gene-copy abundance estimates. The global bacterial co-occurrence network, constructed from 21 bacterial 16S rRNA gene profiles across the full cultivation cycle, is shown in (a), and stage-specific bacterial networks are shown for PBS (b), IES (c), MGS (d), PFS (e), YGS (f), HRS (g), and PRS (h). The global fungal co-occurrence network, constructed from 21 fungal ITS profiles across the full cultivation cycle, is shown in (i), and stage-specific fungal networks are shown for the corresponding stages: PBS (j), IES (k), MGS (l), PFS (m), YGS (n), HRS (o), and PRS (p). The integrated global cross-domain bacterial–fungal co-occurrence network was constructed from 42 microbial profiles, comprising 21 bacterial 16S rRNA gene profiles and 21 fungal ITS profiles derived from the same 21 soil samples across the cultivation cycle (q). The *Morchella*-centered subnetwork highlights ASVs directly or indirectly associated with *Morchella* within the integrated cross-domain network (r). Global networks were used to assess overall domain-specific and cross-domain association structures, whereas stage-specific networks were used to visualize stage-associated changes in network topology. In all panels, nodes represent individual ASVs with prevalence $\geqslant$ 20%, and node sizes are proportional to spike-in-calibrated gene-copy abundance estimates. Edges represent significant Spearman correlations between ASVs ($|\rho| > 0.6$, FDR-adjusted $p < 0.05$). Network topological parameters are shown for each corresponding network.

and fungal communities. Bacterial assemblages formed dense and persistent networks across the cultivation cycle, whereas fungal communities exhibited more variable and stage-sensitive topological structures. Integrated cross-domain networks further indicate that bacterial lineages constitute a major structural backbone of the cultivation microbiome. Together with diversity and community assembly analyses, these patterns suggest that the broader MGS–YGS window, particularly the PFS–YGS transition, represents a period of intensified fungal community restructuring and potential enrichment of risk-associated fungal taxa.

Soil nutrients and moisture are associated with bacterial and fungal community succession

To delineate the environmental drivers associated with microbial succession during *Morchella* cultivation, we coupled temporal monitoring of soil physicochemical properties with Mantel tests, redundancy analysis (RDA), and edaphic correlation networks (Fig. 6). Among the measured edaphic parameters, labile pools of available phosphorus (AP) and available potassium (AK) exhibited pronounced stage-dependent fluctuations, accompanied by temporal variation in moisture content (MC) and total nitrogen (TN). In contrast, alkaline-hydrolyzable nitrogen (AN) showed relatively minor variation, whereas bulk properties—including pH, soil organic matter (SOM), total phosphorus (TP), and total potassium (TK)—remained highly stable. These patterns indicate that temporal environmental variability was primarily associated with fluctuations in labile nutrient pools and water availability, rather than changes in bulk soil properties.

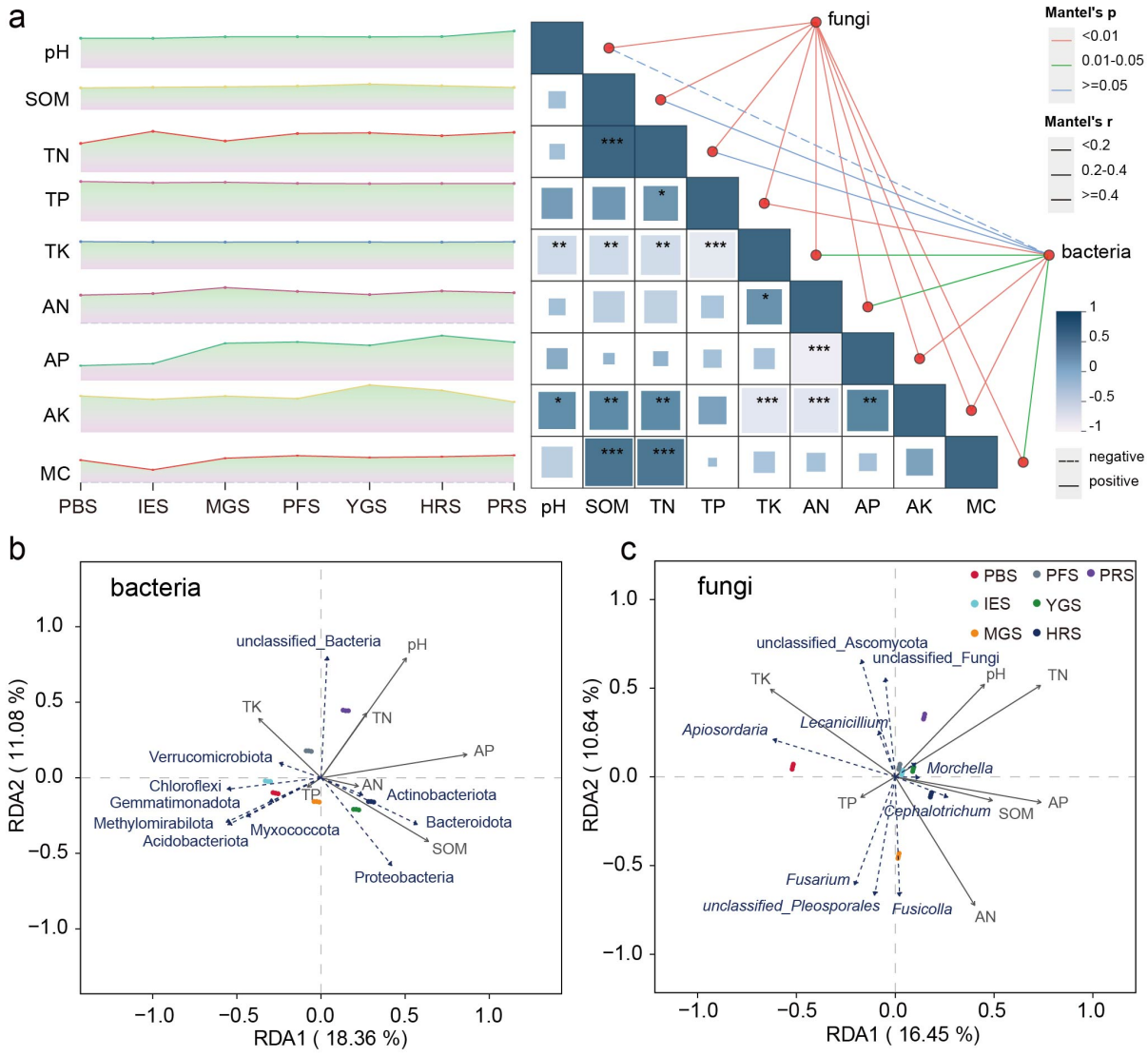

Fig. 6 Associations between soil physicochemical properties and microbial communities. Temporal trajectories of soil physicochemical variables and Mantel-test correlation networks show associations between environmental variation and bacterial or fungal community composition (a). Node size represents Mantel's *r*, and edges indicate significant associations ($p < 0.05$). Edge color denotes the direction of association, with red indicating positive associations and blue indicating negative associations. RDA (redundancy analysis) ordinations for bacterial (b) and fungal (c) communities illustrate relationships between community structure and soil variables. Arrows indicate soil variables significantly associated with community composition based on permutation tests ($p < 0.05$), and centroids represent major bacterial phyla or key fungal genera. Only variables retained after VIF screening are shown.

Non-parametric Mantel tests revealed significant associations ($p < 0.05$) between both bacterial and fungal community structures and multiple soil variables, including pH, AN, AP, AK, and MC (Fig. 6a). Notably, network-based correlation analysis indicated that the fungal domain exhibited broader and stronger associations with these environmental variables than the bacterial domain, suggesting higher environmental responsiveness of the soil mycobiome.

Redundancy analysis (RDA) further resolved domain-specific associations between microbial communities and edaphic gradients (Fig. 6b, c). Bacterial community structure was primarily associated with relatively stable soil properties, including pH, TN, AN, and SOM, with dominant bacterial phyla—such as Proteobacteria, Actinobacteriota, and Acidobacteriota—distributed along these gradients (Fig. 6b). This pattern is consistent with the comparatively stable bacterial community structure observed across the cultivation cycle. In contrast, fungal community composition showed stronger associations with more dynamic environmental variables, particularly AN, AP, MC, and pH (Fig. 6c). Key fungal genera, including *Morchella*, *Lecanicillium*, and *Fusarium*, were distributed along gradients of nutrient availability and moisture, indicating that fungal succession is closely linked to transient changes in soil resource conditions. Specifically, *Morchella* was positively associated with elevated SOM and moderate AP levels, consistent with its increased abundance during reproductive development.

Collectively, these results suggest that temporal microbial succession in *Morchella* cultivation soils is associated with variation in labile nutrients—particularly nitrogen- and phosphorus-related fractions—together with soil moisture. While both bacterial and fungal communities responded to edaphic gradients, the fungal community showed a stronger coupling with dynamic environmental variables. This pattern indicates that fungal communities may serve as more sensitive indicators of short-term environmental variability during *Morchella* cultivation.

Stage-specific fungal succession identifies candidate disease-risk windows in *Morchella* cultivation

Fungal community succession during *Morchella* cultivation followed a host-dominated but stage-sensitive trajectory (Fig. 7). *Morchella* remained a major fungal taxon throughout the cultivation cycle, with its spike-in-calibrated gene-copy abundance increasing during reproductive development, peaking at the Harvest Stage (HRS), and declining sharply during the Post-harvest Recovery Stage (PRS) (Fig. 7b). This pattern indicates the strong dominance of *Morchella* during fruiting and its rapid reduction after harvest.

In contrast, several putative antagonistic or pathogen-associated fungal taxa showed elevated abundance before or during early reproductive development. In particular, *Fusarium* and *Lecanicillium* were enriched during the interval from the Mycelial Growth Stage (MGS) to the Young Fruiting Body Stage (YGS), and their temporal patterns showed negative associations with *Morchella* abundance (Fig. 7b). These dynamics suggest that the MGS–YGS interval may represent a candidate disease-risk window, during which *Morchella* development coincides with increased abundance of potentially antagonistic fungi.

Saprotrophic taxa displayed complementary temporal dynamics. *Mortierella* was abundant during the Pre-sowing Background Stage (PBS) and Initial Establishment Stage (IES) and reappeared during PRS, suggesting potential involvement in early nutrient turnover and post-harvest decomposition. Other saprotrophic or opportunistic genera, including *Chaetomium* and *Nigrospora*, increased during later stages, consistent with a shift toward decomposer-associated fungal succession after harvest (Fig. 7a, b).

Phylogenetic composition further supported these stage-associated patterns (Fig. 7c). Ascomycota was the dominant fungal phylum across the cultivation cycle, with Pezizales, including *Morchella*, markedly enriched at HRS. Hypocreales, including *Fusarium* and *Lecanicillium*, showed higher representation during MGS–PFS, whereas Mortierellomycota was more abundant at PBS, IES, and PRS. These phylogenetic patterns are consistent with three broad successional phases: a candidate risk-associated phase during MGS–YGS, characterized by increased abundance of putative antagonistic or pathogen-associated fungi; a host-dominant phase at HRS, characterized by peak *Morchella* abundance; and a decomposer-resurgence phase at PRS, characterized by increased saprotrophic turnover.

Overall, this stage-resolved analysis highlights the close association between *Morchella* developmental progression and fungal community succession. The enrichment of putative antagonistic taxa during MGS–YGS, together with the dominance of *Morchella* at HRS and saprotrophic resurgence at PRS, provides a temporal framework for identifying candidate disease-risk periods and post-harvest management targets in *Morchella* cultivation systems.

Positive and negative fungal associations highlight a core host-competition window

To further characterize fungal association patterns around *Morchella*, we separated fungal co-occurrence networks into positive and negative associations across developmental stages (Fig. 8). Negative associations between *Morchella* and other fungal taxa were more prominent than positive associations, particularly during the Primordium Formation Stage (PFS) and Young Fruiting Body Stage (YGS). This pattern suggests that fungal community associations during early reproductive development were characterized by intensified competitive or antagonistic signals.

Several putative antagonistic, pathogen-associated, or fast-growing saprotrophic taxa, including *Fusarium*, *Lecanicillium*, *Nigrospora*, and members of Chaetomiaceae, showed negative associations with *Morchella* during PFS–YGS. These taxa also appeared within negative-association subnetworks during the same interval, suggesting that they may contribute to a competitive fungal microenvironment surrounding *Morchella* during primordium formation and early fruiting. In contrast, positive associations with *Morchella* were less frequent and involved fewer taxa, indicating that the native fungal community provided limited positive association signals during these stages.

The predominance of negative fungal associations during PFS–YGS is consistent with the compositional and functional patterns described above, including the enrichment of putative antagonistic or pathogen-associated fungi and the increased representation of mixed trophic guilds during early reproductive development. Together, these results identify

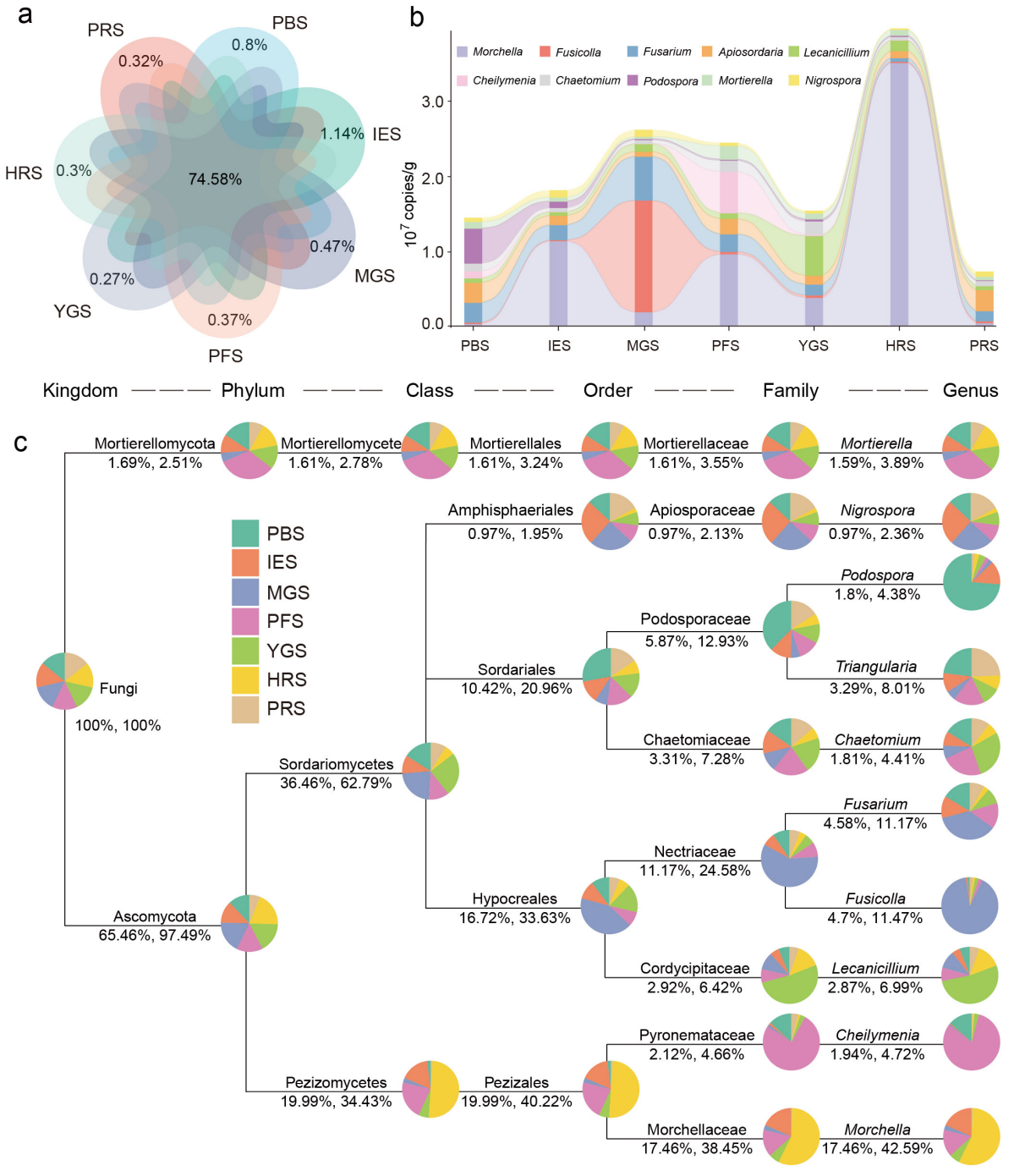

Fig. 7 Stage-specific dynamics and phylogenetic composition of key fungal taxa. The Venn diagram shows shared and stage-specific fungal genera across the seven developmental stages (a). Temporal dynamics of dominant fungal genera based on spike-in-calibrated ITS copy-number abundance estimates (copies g^{-1} dry soil) are shown in (b), including *Morchella*, *Fusicolla*, *Fusarium*, *Apiosordaria*, *Lecanicillium*, *Cheilymenia*, *Chaetomium*, *Podospora*, *Mortierella*, and *Nigrospora*. *Morchella* reached its highest abundance at the Harvest Stage (HRS), whereas several putative antagonistic or pathogen-associated genera, including *Fusarium* and *Lecanicillium*, showed elevated abundance during the broader MGS–YGS candidate disease-risk window, with stronger representation around MGS–PFS. *Mortierella* was abundant during PBS–IES and reappeared at PRS, consistent with early-stage and post-harvest saprotrophic succession. Phylogenetic composition from kingdom to genus is shown in (c) using color-coded pie charts. Ascomycota predominated across stages; Pezizales, including *Morchella*, peaked at HRS; and Hypocreales, including *Fusarium* and *Lecanicillium*, showed higher representation mainly during MGS–PFS and the early reproductive transition.

PFS–YGS as a core host-competition window within the broader MGS–YGS candidate disease-risk period.

Overall, the positive–negative network analysis provides association-based evidence that biotic relationships within the fungal community may contribute to stage-dependent vulnerability during *Morchella* cultivation. These findings suggest that targeted management during PFS–YGS, such as suppressing candidate antagonistic fungi or enhancing beneficial microbial consortia, may help stabilize the fungal microenvironment and improve cultivation outcomes.

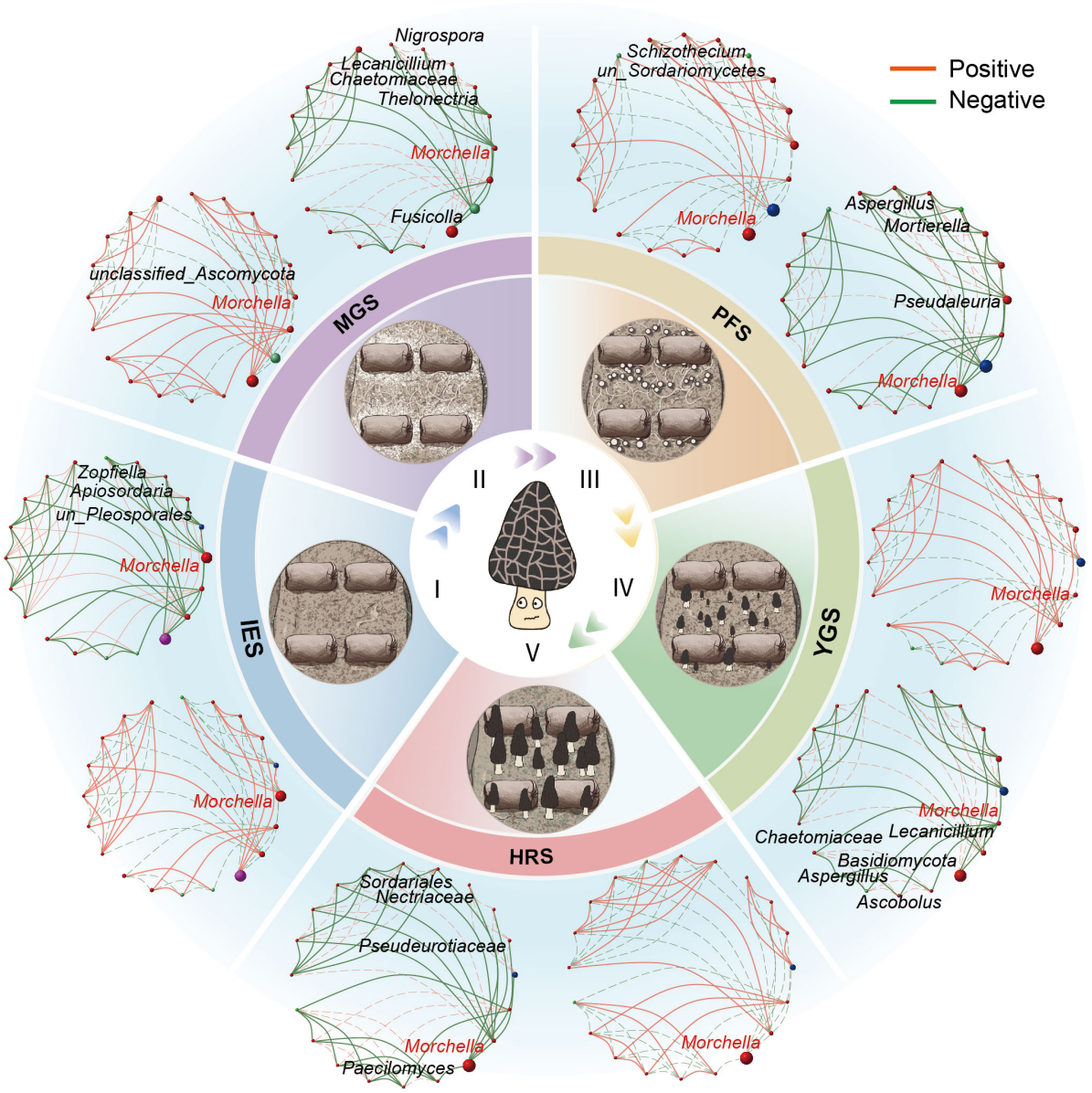

Fig. 8 Stage-specific positive and negative fungal co-occurrence networks. Circular networks illustrate positive and negative associations among dominant fungal taxa across IES, MGS, PFS, YGS, and HRS. Edges represent significant Spearman correlations between fungal taxa ($|\rho| > 0.6$, FDR-adjusted $p < 0.05$), with red indicating positive associations and green indicating negative associations. Node size reflects spike-in-calibrated gene-copy abundance estimates (copies g^{-1} dry soil), and node color indicates taxonomic identity, with *Morchella* highlighted in red. The central panel shows representative developmental stages of *M. sextelata* during cultivation.

Discussion

This study provides a high-resolution, spike-in-calibrated quantitative characterization of soil microbial succession throughout the full cultivation cycle of *Morchella*. Compared with conventional relative-abundance profiling, our spike-in-calibrated approach effectively mitigates compositional constraints inherent in proportional data, revealing pronounced shifts in bacterial 16S rRNA gene and fungal ITS copy-number abundances that would otherwise remain obscured. This distinction is particularly relevant in fungal cropping systems, where host-associated biomass expansion, substrate transformation, and microbial community turnover occur simultaneously. By integrating quantitative abundance profiles with community assembly, co-occurrence network, and environmental association analyses, we provide a coherent ecological framework for interpreting domain-specific microbial dynamics in *Morchella* cultivation soils.

Across the cultivation cycle, bacterial communities exhibited comparatively stable successional dynamics. Bacterial succession was characterized by strong homogeneous selection, cohesive and highly connected co-occurrence networks, and consistent associations with bulk edaphic properties such as pH, soil organic matter (SOM), and total nitrogen (TN). These patterns are consistent with the role of bacterial assemblages as relatively buffered components of host-associated and agricultural soil microbiomes, likely stabilized by functional redundancy and

environmental filtering (Osburn et al. 2019; Ling et al. 2022; Zhu et al. 2022; Kajihara & Hynson 2024). Global-scale studies have similarly shown that the plant–soil interface strongly filters bacterial communities while promoting ecological resilience (Ling et al. 2022). In our study, bacterial stability was closely associated with pH, TN, and SOM, suggesting that relatively stable edaphic properties may contribute to maintaining bacterial community coherence during *Morchella* cultivation.

In contrast, fungal communities showed pronounced stage-dependent restructuring during reproductive development. The PFS and YGS stages were associated with elevated fungal compositional turnover, more variable βNTI patterns, and increased network fluctuations, indicating that the soil mycobiome is more responsive to developmental-stage transitions than the bacterial community. This pattern is consistent with ecological expectations that host developmental transitions or stress-associated states can increase microbial variability, in line with the Anna Karenina principle, which describes increased heterogeneity in disturbed or dysbiotic microbiomes (Zaneveld et al. 2017). Similar stage-linked instability has been reported in diverse edible mushroom systems, including *Agaricus bisporus* (Berendsen et al. 2010; Banks et al. 2019; Ban et al. 2023), *Lentinula edodes* (Wang et al. 2016; An et al. 2022; Cao et al. 2024), and *Pleurotus ostreatus* (Innocenti et al. 2019). In particular, microbial succession during button mushroom production further supports the view that stage-associated microbial turnover is a common ecological feature of intensive edible mushroom cultivation systems (Ban et al. 2023). Together, these findings indicate that host developmental stage is a major factor associated with fungal community restructuring in mushroom cultivation systems. However, the underlying mechanisms, such as shifts in host carbon allocation, substrate utilization, or exudation profiles, remain to be validated through metabolomic and transcriptomic approaches.

The enrichment of putative antagonistic or pathogen-associated fungal taxa during early reproductive development suggests that the MGS–YGS interval may represent a candidate disease-risk window, with PFS–YGS forming a core phase of intensified fungal association changes. In particular, *Fusarium* and *Lecanicillium* were repeatedly detected during this interval, showing temporal patterns associated with fungal community restructuring. Although the present study did not experimentally confirm pathogenicity, these taxa are ecologically relevant because members of these genera have been linked to disease or antagonistic interactions in mushroom systems. For example, *Lecanicillium fungicola* is the causal agent of dry bubble disease in *Agaricus bisporus*, where infection incidence and symptom severity are associated with host developmental stages (Berendsen et al. 2010; Banks et al. 2019; Quiroz et al. 2024). In *Morchella*, white mold disease caused by *Paecilomyces penicillatus* has been confirmed by Koch's postulates and is prevalent in major production regions (He et al. 2017). *Fusarium* has also been reported as a causal agent of stipe rot and white mold diseases in cultivated morels, including diseases associated with the *Fusarium incarnatum–Fusarium equiseti* species complex and *Fusarium nematophilum* (Guo et al. 2016; Liu et al. 2021; Wang et al. 2026). Similarly, *Lecanicillium aphanocladii* has been reported to cause rot disease of *Morchella sextelata* in China (Lv et al. 2022). These observations suggest that the recurrent enrichment of putative antagonistic or pathogen-associated fungi may serve as a potential early indicator of community destabilization prior to visible disease symptoms.

Because the *Morchella* cultivation system was based on loamy soil amended with wheat straw and organic fertilizer, substrate-derived carbon availability and microbial immigration may have contributed to the observed stage-associated fungal turnover. This interpretation is consistent with observations from *Agaricus bisporus* compost systems, where straw-based compost substrates were shown to shape microbial assembly and successional trajectories during mushroom production (Qian et al. 2025). Therefore, the enrichment of *Fusarium* and *Lecanicillium* during the MGS–YGS interval may reflect not only host developmental transitions but also substrate-associated ecological filtering and resource-driven niche shifts. However, because this study did not directly trace substrate-derived microorganisms or quantify microbial immigration from wheat straw and organic fertilizer, the contribution of substrate-associated inocula remains an important hypothesis requiring future validation through substrate sterilization, source-tracking, and controlled inoculation experiments.

By integrating the abundance dynamics of these candidate risk-associated taxa with βNTI-derived assembly patterns and network associations, this study provides a basis for identifying vulnerable developmental periods in *Morchella* cultivation. Stage-associated disease-risk windows appear to be common across edible fungi. In *Agaricus bisporus*, dry bubble disease typically occurs when the casing layer is colonized but primordia have not yet formed (Berendsen et al. 2010; Banks et al. 2019), representing a well-documented infection window. In *Lentinula edodes*, green mold caused by *Trichoderma* spp. frequently disrupts fruiting initiation, although the precise most vulnerable stage remains to be fully resolved (Wang et al. 2016; An et al. 2022; Cao et al. 2024). Similarly, in *Pleurotus ostreatus*, *Trichoderma*-associated blight often emerges during substrate colonization and occasionally during fruiting, suggesting stage-dependent risks, though the evidence remains largely correlative (Innocenti et al. 2019). Together, these examples suggest that developmental transitions may represent ecological vulnerability windows in mushroom cultivation systems.

The contrasting assembly patterns of bacterial and fungal communities further highlight domain-specific ecological roles in *Morchella* cultivation soils. Bacterial communities displayed abundance–occurrence patterns partly consistent with neutral expectations while maintaining strong signals of homogeneous selection. This pattern suggests that neutral-like abundance distributions may emerge within an environmentally filtered bacterial pool, consistent with the concept that phylogenetic conservatism and functional redundancy contribute to bacterial community stability (Kajihara & Hynson 2024). Fungal communities, in contrast, showed weaker support for neutral assembly and stronger stage-associated restructuring, particularly during reproductive transitions. From a management perspective, this divergence suggests that bacterial communities may provide a relatively stable background microbiome, whereas fungal communities may serve as more sensitive indicators of cultivation-stage transitions and candidate disease-risk development.

Environmental association analyses further suggested that fungal succession was more strongly coupled with labile edaphic factors, particularly available phosphorus, available potassium, and moisture content, than with relatively stable bulk soil properties. These variables may influence fungal competition by modifying nutrient accessibility, hyphal growth conditions, and microhabitat heterogeneity during the transition from vegetative growth to reproductive development. This interpretation is consistent with studies showing that mushroom-derived organic amendments, including spent mushroom substrate, can alter soil nutrient availability and microbial community composition (Yang G et al. 2024). Together, these findings support the view that substrate history, labile nutrient pools, and moisture dynamics are important ecological filters shaping cultivation-soil mycobiomes. Nevertheless, because the present study was observational, these edaphic associations should be interpreted as ecological correlations rather than direct causal effects.

These findings have practical implications for microbiome-informed management of *Morchella* cultivation systems. The candidate disease-risk window identified here, particularly the broader MGS–YGS interval and the core PFS–YGS transition, represents a key period for targeted intervention. Potential strategies include optimizing nutrient and moisture conditions—particularly phosphorus, potassium, and water availability—and introducing beneficial microorganisms capable of suppressing antagonistic fungi or stabilizing the fungal microenvironment. The potential contribution of substrate-associated microbial inputs also suggests that wheat straw quality, organic fertilizer source, composting status, and pre-treatment procedures may influence disease-risk development. In plant microbiome management, synthetic community (SynCom) inoculation strategies have been shown to enhance host resilience (Toju et al. 2018). Likewise, *Pseudomonas chlororaphis* has been validated in field experiments for its antagonistic activity against white mold in morel cultivation (Yu et al. 2025). However, extending these strategies across cultivation systems will require careful consideration of site-specific soil properties, substrate history, microbial background communities, and environmental variability.

This study positions *Morchella* cultivation soils as a valuable model system for investigating microbial community assembly under the combined influence of host development, substrate transformation, and environmental filtering. By identifying candidate disease-risk developmental windows characterized by fungal community restructuring, network association changes, and enrichment of taxa frequently linked to antagonistic interactions, we propose a quantitative framework that integrates microbial profiling with community assembly and environmental association analyses. This framework aligns with emerging paradigms in agricultural ecology that emphasize the balance between ecosystem stability and functional plasticity (Banerjee & van der Heijden 2023).

Despite these advances, several limitations should be acknowledged. First, the study was conducted at a single geographic location and during one cultivation cycle, which may limit the generalizability of the observed microbial dynamics across broader agroclimatic contexts. Second, although spike-in calibration reduces compositional bias (Vandeputte et al. 2017; Boshier et al. 2020), two technical constraints remain: synthetic DNA may differ from native microbial DNA in extraction or amplification efficiency, and 16S rRNA gene and ITS copy-number variation among taxa was not corrected. Therefore, our estimates should be interpreted as spike-in-calibrated gene-copy abundance estimates rather than absolute microbial cell numbers. Third, the evidence presented here remains largely correlative. In particular, Koch's postulates or inoculation-based validation were not performed to confirm whether the detected *Fusarium* and *Lecanicillium* ASVs directly contribute to disease development. Thus, these taxa should be regarded as candidate risk-associated fungi rather than confirmed causal agents. Fourth, although substrate-derived carbon availability and microbial immigration may contribute to fungal community succession, this study did not directly characterize the microbiota of wheat straw, organic fertilizer, or other cultivation inputs. Finally, strain-level functional heterogeneity, which may be critical for host–microbe interactions, was not resolved by amplicon sequencing.

Future work should employ multi-site and multi-year designs to test the robustness of these microbial transitions under diverse environmental and management conditions. Integrating spike-in-calibrated quantification with βNTI-based assembly inference, multi-omics profiling, including metagenomics, metatranscriptomics, and metabolomics, and synthetic community reconstruction will be essential for bridging correlation and causation (Lutz et al. 2023; Deng et al. 2025b). Future substrate-tracing experiments that compare different straw sources, organic fertilizer inputs, composting regimes, and pre-treatment strategies will also be important for determining how cultivation substrates influence microbial immigration, fungal competition, and disease-risk development. Such integrative approaches will advance mechanistic understanding of microbiome dynamics in host-managed fungal cropping systems and support precision microbiome management strategies aimed at improving host resilience, reducing disease risk, and stabilizing yield outcomes.

Conclusions

This study applied spike-in-calibrated amplicon sequencing to resolve bacterial and fungal community succession across the full cultivation cycle of *Morchella*. This approach provides a more quantitative perspective on microbial dynamics by mitigating the compositional constraints inherent in relative-abundance data and enabling gene-copy-level inference across both bacterial and fungal domains. Our results show that bacterial communities maintain relatively stable, environmentally structured assemblages, primarily associated with homogeneous selection and stable edaphic properties, including pH, soil organic matter, and total nitrogen. In contrast, fungal communities exhibit pronounced stage-dependent restructuring, particularly during reproductive development. The broader MGS–YGS interval, with a core transition during PFS–YGS, is characterized by elevated fungal network variability and enrichment of putative antagonistic or pathogen-associated taxa, including *Fusarium* and *Lecanicillium*, suggesting a potential disease-risk window. Together, these findings support the view that host developmental transitions represent key ecological axes shaping fungal community instability and potential vulnerability periods in *Morchella* cultivation soils. By integrating spike-

in-calibrated gene-copy abundance estimates with community assembly patterns, co-occurrence networks, and taxon-level diagnostics, this study establishes a quantitative ecological framework for identifying disease-risk windows and informing microbiome-guided management strategies. Future work incorporating multi-site and multi-year sampling, targeted inoculation experiments, and multi-omics approaches will be essential to validate causal mechanisms and extend these findings toward predictive and precision microbiome management in commercial mushroom cultivation systems.

Acknowledgments

This work was supported by the earmarked fund for China Agriculture Research System (CARS-20), the China Agriculture Research System—Sichuan Edible Fungi Innovation Team (SCCXTD-2024-7), and the Sichuan Science and Technology Program (2025ZNSFSC0991).

Author contributions

Xie LY conceived the project. Chen Y, Deng ZL, and Xie LY designed the experiments. Cao XL, Chen Y, Xie LY, and Deng ZL coordinated field sampling across seven cultivation stages and measured soil physicochemical properties. Chen Y and Deng ZL carried out high-throughput sequencing. Liu SS, Liu LX, Tang J, Wang XR, Li TL, and Tian C assisted with field sample collection and sequencing. Deng ZL and Ou J conducted bioinformatic, ecological, and statistical analyses and curated the data. Deng ZL, Tang J, and Xie LY interpreted the data and wrote the manuscript with input from all authors. All authors approved the final manuscript.

ORCID

Ying Chen: https://orcid.org/0009-0007-7743-8851
Li-Yuan Xie: https://orcid.org/0000-0002-6176-0340

Conflict of interest statement

All authors declare that they have no competing interests.

Data availability statement

All data generated or analyzed in this study are included in the article. Additional information is available from the corresponding authors upon request.

Supplementary Information

The online version contains supplemental information available at https://doi.org/10.65390/fdiv.2026.136017.

References

An XY, Cheng GH, Gao HX, Li XF, Yang Y, Li D, Li Y (2022) Phylogenetic analysis of *Trichoderma* species associated with green mold disease on mushrooms and two new pathogens on *Ganoderma sichuanense*. Journal of Fungi 8(7):704. https://doi.org/10.3390/jof8070704

Ban GH, Kim JH, Kim SA, Rhee MS (2023) Microbial succession during button mushroom (*Agaricus bisporus*) production evaluated via high-throughput sequencing. Food Microbiology 114:104307. https://doi.org/10.1016/j.fm.2023.104307

Banerjee S, van der Heijden MGA (2023) Soil microbiomes and one health. Nature Reviews Microbiology21(1):6–20. https://doi.org/10.1038/s41579-022-00779-w

Banks AM, Aminuddin F, Williams K, Batstone T (2019) Genome sequence of *Lecanicillium fungicola* 150-1, the causal agent of dry bubble disease. Microbiology Resource Announcements 8(19):e00340-19. https://doi.org/10.1128/MRA.00340-19

Benucci GMN, Longley R, Zhang P, Zhao Q, Bonito G (2019) Microbial communities associated with the black morel *Morchella sextelata* cultivated in greenhouses. PeerJ 7:e7744. https://doi.org/10.7717/peerj.7744

Berendsen RL, Baars JJP, Kalkhove SIC, Lugones LG, Wösten HAB, Visser J (2010) *Lecanicillium Fungicola*: causal agent of dry bubble disease in white-button mushroom. Molecular Plant Pathology 11(5):585–595. https://doi.org/10.1111/j.1364-3703.2010.00627.x

Boshier FAT, Srinivasan S, Lopez A, Hoffman NG, Herbst-Kralovetz MM (2020) Complementing 16S rRNA gene amplicon sequencing with total bacterial load to infer absolute species concentrations in the vaginal microbiome. mSystems 5(2):e00777-19. https://doi.org/10.1128/mSystems.00777-19

Cao ZJ, Zhao J, Liu Y, Wang SX, Chen Y, Wang Y (2024) Diversity of *Trichoderma* species associated with green mold contaminating substrates of *Lentinula edodes* and their interaction. Frontiers in Microbiology 14:1288585. https://doi.org/10.3389/fmicb.2023.1288585

Chen X, Zhang Y, Chao S, Song L, Tang J, Li H (2024) Biocontrol potential of endophytic *Bacillus subtilis* A9 against rot disease of *Morchella esculenta*. Frontiers in Microbiology 15:1388669. https://doi.org/10.3389/fmicb.2024.1388669

Cole JR, Wang Q, Cardenas E, Fish J, Chai B, Farris RJ, Kulam-Syed-Mohideen AS, McGarrell DM, Marsh T, Garrity GM, et al (2009) The Ribosomal Database Project: improved alignments and new tools for rRNA analysis. Nucleic Acids Research 37: D141–D145. https://doi.org/10.1093/nar/gkn879

Deng ZL, Dissanayake AJ, Zhu JT, Wu N, Deng J, Du HZ, Li WL, Lu YH, Tang X, Xu JP, et al (2025a) Genomic evolution and diversity in Botryosphaeriales: insights from pan-genomic and population genetic analyses of representative species. Fungal Diversity 134:1–18. https://doi.org/10.1007/s13225-025-00565-y

Deng ZL, Yu FM, Ma X, Zhao Q, Liu JK (2025b) Metagenomic insights into disease-induced microbial dysbiosis and elemental cycling alterations in *Morchella* cultivation soils: evidence from two distinct regions. Journal of Fungi 11(9):663. https://doi.org/10.3390/jof11090663

Doyle B, Reynolds GZM, Dvorak M, Maghini DG, Natarajan A, Bhatt AS (2025) Absolute quantification of prokaryotes in the microbiome by 16S rRNA qPCR or ddPCR. Nature Protocols 20:3441–3476. https://doi.org/10.1038/s41596-025-01165-5

Du XH, Yang ZL (2021) Mating systems in true morels (*Morchella*). Microbiology and Molecular Biology Reviews 85(3):e00220-20. https://doi.org/10.1128/MMBR.00220-20

Guo MC, Wu BC, Luo CY, Sa W, Liu TH, Yu Y (2025) The effects of fungal pathogen infestation on soil microbial communities for *Morchella sextelata* cultivation on the Qinghai-Xizang Plateau. Journal of Fungi 11(4):264. https://doi.org/10.3390/jof11040264

Guo MP, Chen K, Wang GZ, Bian YB (2016) First report of stipe rot disease on *Morchella importuna* caused by *Fusarium incarnatum–Fusarium equiseti* species complex in China. Plant Disease 100(12):2530. https://doi.org/10.1094/PDIS-05-16-0633-PDN

He P, Geng L, Mao D, Xu C (2012) Production, characterization and antioxidant activity of exopolysaccharides from submerged culture of *Morchella crassipes*. Bioprocess and Biosystems Engineering 35(8):1325–1332. https://doi.org/10.1007/s00449-012-0720-6

He XL, Peng WH, Miao RY, Tang J, Huang Q (2017) White mold on cultivated morels caused by *Paecilomyces penicillatus*. FEMS Microbiology Letters364(5):fnx037. https://doi.org/10.1093/femsle/fnx037

Huang K, Li L, Wu W, Pu K, Zhang Y, Wang Y (2024) Enhancing morel yield and quality through the amendment of soil physicochemical properties and microbial community with wood ash. Microorganisms 12(12):2406. https://doi.org/10.3390/microorganisms12122406

Innocenti G, Montanari M, Righini H, Roberti R (2019) *Trichoderma* species associated with green mould disease of *Pleurotus ostreatus* and their sensitivity to prochloraz. Plant Pathology 68(2):392–398. https://doi.org/10.1111/ppa.12953

Kajihara KT, Hynson NA (2024) Networks as tools for defining emergent properties of microbiomes and their stability. Microbiome12(1):1868. https://doi.org/10.1186/s40168-024-01868-z

Kewlani P, Tiwari D, Singh L, Balodi S, Bhatt ID (2023) Food and antioxidant supplements with therapeutic properties of *Morchella esculenta* (Ascomycetes): a review. International Journal of Medicinal Mushrooms25(9):11–29. https://doi.org/10.1615/IntJMedMushrooms.2023049147

Li Y, Lin W, Chen J, Lin J, Liu Y, Pu K (2024) Nitrates and microbiome components engaged in denitrification within soil regulate *Morchella* spp. growth. Horticulturae10(9):905. https://doi.org/10.3390/horticulturae10090905

Ling N, Wang T, Kuzyakov Y (2022) Rhizosphere bacteriome structure and functions. Nature Communications 13(1):28448. https://doi.org/10.1038/s41467-022-28448-6

Liu C, Sun Y, Mao Q, Guo X, Li P, Liu Y, Xu N (2016) Characteristics and antitumor activity of *Morchella esculenta* polysaccharide extracted by pulsed electric field. International Journal of Molecular Sciences17(6):986. https://doi.org/10.3390/ijms17060986

Liu Q, Ma H, Zhang Y, Dong C (2018) Artificial cultivation of true morels: current state, issues and perspectives. Critical Reviews in Biotechnology 38(2):259–271. https://doi.org/10.1080/07388551.2017.1333082

Liu S, He Y, Fan T, Zhu M, Qi C, Ma Y, Yang M, Yang L, Tang X, Zhou J, et al (2024) PAM-relaxed and temperature-tolerant CRISPR-Mb3Cas12a single transcript unit systems for efficient singular and multiplexed genome editing in rice, maize, and tomato. Plant Biotechnology Journal 23(1):156–173. https://doi.org/10.1111/pbi.14486

Liu TH, Yu Y, Kang X, Liu T, Wang Y, Tan H (2021) A new stipe rot disease of the cultivated *Morchella sextelata*. Mycosystema 40:2229–2243. https://doi.org/10.13346/j.mycosystema.210055

Lutz S, Bodenhausen N, Hess J, Valzano-Held A, van der Heijden MGA (2023) Soil microbiome indicators can predict crop growth response to large-scale inoculation with arbuscular mycorrhizal fungi. Nature Microbiology8(12):2277–2289. https://doi.org/10.1038/s41564-023-01520-5

Lv BB, Yu S, Chen YF, Yu HL, Huang Q (2022) First report of *Lecanicillium aphanocladi* causing rot of *Morchella sextelata* in China. Plant Disease 106(12):3202. https://doi.org/10.1094/PDIS-12-21-2656-PDN

Ning D, Deng Y, Tiedje JM, Zhou J (2019) A general framework for quantitatively assessing ecological stochasticity. Proceedings of the National Academy of Sciences of the United States of America 116(34):16892–16898. https://doi.org/10.1073/pnas.1904623116

Orlofsky E, Zabari L, Bonito G, Masaphy S (2021) Changes in soil bacteria functional ecology associated with *Morchella rufobrunnea* fruiting in a natural habitat. Environmental Microbiology23(11):6651–6662. https://doi.org/10.1111/1462-2920.15692

Osburn ED, McBride SG, Aylward FO, Badgley BD, Strahm BD (2019) Soil bacterial and fungal communities exhibit distinct long-term responses to disturbance in temperate forests. Frontiers in Microbiology 10:2872. https://doi.org/10.3389/fmicb.2019.02872

Pion M, Spangenberg JE, Simon A, Bindschedler S, Chatzinotas A, Job D, Zenobi R, Flury B, Aragno M, Meylan W, Rasmann S, Sanders IR (2013) Bacterial farming by the fungus *Morchella crassipes*. Proceedings of the Royal Society B: Biological Sciences 280(1773):20132242. https://doi.org/10.1098/rspb.2013.2242

Qian K, Dong P, Alim A, Li Y, Wang Y, Liu Y (2025) Microbial community succession patterns and assembly mechanisms in the white button mushroom (*Agaricus bisporus*) production with corn straw-based compost. Environmental Technology & Innovation38:104135. https://doi.org/10.1016/j.eti.2025.104135

Quast C, Pruesse E, Yilmaz P, Gerken J, Schweer T, Yarza P, Peplies J, Glöckner FO (2013) The SILVA ribosomal rRNA gene database project: improved data processing and web-based tools. Nucleic Acids Research 41(D1):D590–D596. https://doi.org/10.1093/nar/gks1219

Quiroz LF, Ciosek T, Grogan H, McKeown PC, Jones PW, Kavanagh K (2024) Unravelling the transcriptional response of *Agaricus bisporus* under *Lecanicillium fungicola* infection. International Journal of Molecular Sciences 25(2):1283. https://doi.org/10.3390/ijms25021283

R Core Team (2022) R: A language and environment for statistical computing. R Foundation for Statistical Computing, Vienna, Austria. https://www.R-project.org/

Stegen JC, Lin X, Fredrickson JK, Chen X, Kennedy DW, Murray CJ, Rockhold ML, Konopka A (2013) Quantifying community assembly processes and identifying features that impose them. The ISME Journal 7(11):2069–2079. https://doi.org/10.1038/ismej.2013.93

Tan H, Liu T, Yu Y, Tang J, Wang Y, Peng B (2021) Morel production related to soil microbial diversity and evenness. Microbiology Spectrum 9(2):e00229-21. https://doi.org/10.1128/Spectrum.00229-21

Toju H, Peay KG, Yamamichi M, Narisawa K, Hiruma K, Fukuda S, Ushio M, Nakaoka S, Yoshida K, Schlaeppi K, Minamisawa K, Kiers ET (2018) Core microbiomes for sustainable agroecosystems. Nature Plants 4(5):247–257. https://doi.org/10.1038/s41477-018-0139-4

Tourlousse DM, Yoshiike S, Ohashi A, Matsukura S, Narita S, Miura T, Morita S, Noda N (2017) Synthetic spike-in standards for high-throughput 16S rRNA gene amplicon sequencing. Nucleic Acids Research 45(4):e23. https://doi.org/10.1093/nar/gkw983

Vandeputte D, Kathagen G, D'hoe K, Vieira-Silva S, Valles-Colomer M, Wang J, Tito RY, De Commer L, Darzi Y, Falony G, Raes J (2017) Quantitative microbiome profiling links gut community variation to microbial load. Nature 551:507–511. https://doi.org/10.1038/nature24460

Wang G, Cao X, Ma X, Guo M, Zhao Q, Liu TH, Yu Y (2016) Diversity and effect of *Trichoderma* spp. associated with green mold disease on *Lentinula edodes* in China. Microbiology Open 5(4):709–718. https://doi.org/10.1002/mbo3.364

Wang L, Zhao Q, Bai M, Wang Y, Liu TH, Yu Y (2026) Identification and characterization of pathogenic *Fusarium* species causing white mold disease in cultivated morels (*Morchella* spp.) in China. Journal of Fungi 12(3):184. https://doi.org/10.3390/jof12030184

Wu H, Chen J, Li J, Liu Y, Yang L, Xu C, Li Y (2021) Recent advances on bioactive ingredients of *Morchella esculenta*. Applied Biochemistry and Biotechnology 193(12):4197–4213. https://doi.org/10.1007/s12010-021-03670-1

Xu L, Zhang Y, Li H, Li J, Liu Y, Pu K (2024) Challenges and strategies for continuous cropping of *Morchella* spp.: a review. Horticulturae 10(12):1288. https://doi.org/10.3390/horticulturae10121288

Yan Q, Wang P, Liu Z, Yu Y, Liu TH (2025a) Analysis of soil microbial community structure and function in *Morchella esculenta* habitats in Jilin Province. Agronomy 15(1):15. https://doi.org/10.3390/agronomy15010015

Yan Q, Wang P, Liu Z, Yu Y, Liu TH (2025b) High-throughput sequencing uncovers fungal community succession during *Morchella sextelata* development. Journal of Fungi 11(5):364. https://doi.org/10.3390/jof11050364

Yang G, Ma Y, Ma X, Wang X, Liu TH, Yu Y (2024) Changes in soil organic carbon components and microbial community following spent mushroom substrate application. Frontiers in Microbiology15:1351921. https://doi.org/10.3389/fmicb.2024.1351921

Yang L, Lou J, Wang H, Wu L, Duan M, Yang Y, Zhang Y, Xu J (2018) Use of an improved high-throughput absolute abundance quantification method to characterize soil bacterial community and dynamics. Science of The Total Environment 633:360–371. https://doi.org/10.1016/j.scitotenv.2018.03.201

Yu FM, Jayawardena RS, Thongklang N, Lv ML, Zhao Q, Liu TH, Yu Y (2022) Morel production associated with soil nitrogen-fixing and nitrifying microorganisms. Journal of Fungi 8(3):299. https://doi.org/10.3390/jof8030299

Yu Y, Kang X, Liu T, Wang Y, Ke YH, Marzani K, Bouazar M, Ghasemi H, Bakhshi E, Khodadadi Manesh S, et al (2025) Inoculation of the *Morchella importuna* mycosphere with *Pseudomonas chlororaphis* alleviated a soil-borne disease caused by *Paecilomyces Penicillatus*. Biology and Fertility of Soils61(1):141–161. https://doi.org/10.1007/s00374-024-01874-1

Yue Y, Hao H, Wang Q, Xiao T, Liu TH, Yu Y (2024) Dynamics of the soil microbial community associated with *Morchella* cultivation: diversity, assembly mechanism and yield prediction. Frontiers in Microbiology 15:1345231. https://doi.org/10.3389/fmicb.2024.1345231

Zaneveld JR, McMinds R, Thurber RV (2017) Stress and stability: applying the Anna Karenina principle to animal microbiomes. Nature Microbiology 2(9):17121. https://doi.org/10.1038/nmicrobiol.2017.121

Zhang C, Shi X, Zhang J, Zhang Y, Liu TH, Yu Y (2023a) Dynamics of soil microbiome throughout the cultivation life cycle of morel (*Morchella sextelata*). Frontiers in Microbiology 14:979835. https://doi.org/10.3389/fmicb.2023.979835

Zhang J, Zhao J, Liu G, Li Y, Wang Y, Liu TH, Yu Y (2023b) Advance in *Morchella* sp. polysaccharides: isolation, structural characterization and structure–activity relationship: a review. International Journal of Biological Macromolecules 247:125819. https://doi.org/10.1016/j.ijbiomac.2023.125819

Zhu J, Niu W, Zhang Z, Siddique KHM, Liu TH, Yu Y (2022) Distinct roles for soil bacterial and fungal communities associated with the availability of carbon and phosphorus under aerated drip irrigation. Agricultural Water Management 274:107922. https://doi.org/10.1016/j.agwat.2022.107922